Mon. Not. R. Astron. Soc. **000**, 000–000 (0000) Printed 2 February 1999 (MN LATEX style file v1.4)

Soft X–ray spectral variations of the narrow line Seyfert 1 galaxy Markarian 766

M. J. Page[1], F. J. Carrera[1,2], J.P.D. Mittaz[1], K.O. Mason[1]
[1]*Mullard Space Science Laboratory, University College London, Holmbury St Mary, Dorking, Surrey RH5 6NT, UK.*
[2]*Instituto de Física de Cantabria (Consejo Superior de Investigaciones Científicas–Universidad de Cantabria), 39005 Santander, Spain.*

ABSTRACT

The X–ray variability of the narrow line Seyfert 1 galaxy Markarian 766 is studied using 9 *ROSAT* PSPC datasets. The spectrum is well described by a power law combined with a blackbody (kT $\sim$ 70 eV) soft excess. Examination of flux ratio changes and variability amplitude in 3 X–ray bands, shows that the power law component varies continuously on time-scales of $\sim 5000s$ and is steeper when it is brighter. In contrast, variability of the soft excess is *not* detected. Spectral modeling of 31 spectra from different observations and at a range of count rates is also consistent with a picture in which the power law is steeper when it is brighter, and in which the soft excess component does not vary. The power law variability can be explained if the power law is produced by variable thermal or non-thermal Comptonization of soft photons. This behaviour is similar to that of Galactic black hole candidates in the low state. The X–ray and multiwavelength properties of Markarian 766 are shown to be very similar to those of other narrow line Seyfert 1s. This may mean that the rapid X–ray variability seen in other narrow line Seyfert 1s may also not originate in their strong soft excess components.

Key words: X–rays:Seyferts - variation:spectral - variation:rapid

1 INTRODUCTION

Studying the X–ray emission from active galactic nuclei allows us to probe deep into their central regions, at scales of a few light minutes to a few light days from the central engine. Timing and spectroscopy of the X–ray emission therefore allow us to examine the conditions and environment in which matter accretes onto a massive black hole.

Of particular importance is the soft X–ray band (0.1 – 2 keV) which has been made accessible by *ROSAT*. Two principal emission components are found in AGN spectra in this band, a power law which extends to much higher energies ($>$ 40 keV) and an excess at low energies (typically $<$ 0.5 keV). This soft excess may be the high energy tail of the big blue bump, which dominates the bolometric luminosity of most radio quiet AGN (e.g. Walter & Fink 1993, Turner & Pounds 1989). Understanding the mechanism by which the soft excess is produced is therefore essential for the construction of a realistic model of the central regions of AGN.

1.1 Models of the X–ray Power Law and Soft Excess

In radio loud AGN, the mechanism responsible for the hard power law is probably synchrotron or synchrotron self Compton radiation from relativistic jets (Shastri et al. 1993). This may not be the case for the power law component seen in the X–ray spectra of radio quiet AGN, which are in general softer than those from radio loud objects (Lawson et al. 1992). At >5 keV, radio quiet AGN show spectral features (Fe line emission and a hardening of the spectrum above 10 keV, Pounds et al. 1990) which suggest that some of the X–rays are reflected from material near the black hole; in MCG-6-30-15 and other Seyfert 1s for which high signal to noise *ASCA* data are available, the Fe line is relativistically broadened (Nandra et al. 1997). Therefore, the X–ray power law component may originate in a hot corona above a relativistic accretion disk so that $\sim$ 50% of the X–rays generated in the corona shine down on the accretion disk, and are reflected from its surface. In this model the X–ray power law may be due to photons which are emitted originally from the accretion disk itself, and then Compton upscattered either by electrons in a hot plasma (Walter & Courvoisier 1992), or by a non-thermal distribution of relativistic electrons injected into a compact region, in which the radiation density may be so high that photon - photon collisions result in production of electron - positron pairs (Zdziarsky et al. 1990).

A number of models have been put forward to explain the soft excess emission of AGN. One obvious model is that the soft excess (and the whole of the big blue bump) is thermal emission from an accretion disk surrounding a supermassive black hole (e.g. Ross, Fabian and Mineshige 1992). Alternatively, the soft excess may be due to reprocessing of the power law component by optically thin clouds that surround the central regions (e.g. Guilbert & Rees 1988), or the surface of an accretion disk (e.g. Ross & Fabian 1993). Reprocessing of the radiation by electron - positron pairs can also produce a soft excess (Zdziarski et al. 1990). In the reprocessing models, the soft excess responds to changes in the power law flux, with a time delay related to the distance between the power law emitter and the reprocessing material. If the power law component is caused by Compton upscattering of soft X–ray and UV accretion disk photons, and accretion disk instabilities drive the variability, then the delay between the power law and soft excess components is expected to be in the opposite sense, i.e. the soft excess changes before the power law component. If the soft excess is due to reprocessing of X–rays by electron - positron pairs, time delays between the power law component and soft excess depend on the compactness of the emission region (Done & Fabian 1989).

1.2 The Narrow Line Seyfert 1 Galaxy Markarian 766

Narrow line Seyfert 1 galaxies (NLS1s hereafter) are known to have strong soft excesses, (Puchnarewicz et al. 1992, Boller, Brandt & Fink 1996) and are therefore obvious candidates for investigating the interrelation between the power law and soft excess components. However, detailed studies of individual objects have tended to concentrate on those with extreme properties, of either abnormally steep soft X–ray spectra and/or unusually large variability, e.g. RE J1034+393 (Puchnarewicz et al. 1995), IRAS 13224-3809 (Otani et al. 1996), RE J1237+264 (Brandt, Pounds & Fink 1995).

In this paper we present a study of the X–ray emission of the nearby (z=0.013), radio quiet, NLS1 galaxy Markarian 766. Markarian 766 fell within the field of view of the *ROSAT* PSPC during 9 different observations, was observed at least once in each of the years 1991 to 1994 inclusive, and is a bright PSPC source (1 – 6 counts s^{-1}). The long sampling time scale provides a rare opportunity to study *both* the long and short term behaviour of the source.

Markarian 766 has a significant but not *extreme* soft excess (Boller, Brandt & Fink 1996), and is known to vary in a few hours (Molendi, Maccacaro & Schaeidt 1993); these are essential properties if the relations between the soft excess and power law components are to be investigated within the time scales of individual *ROSAT* observations. It is a strong Fe II emitter (González-Delgado & Pérez 1996) and has significant optical polarization of $> 2\%$ perpendicular to its radio axis (Goodrich 1989).

Results from some *ROSAT* observations of Markarian 766 have already been published. Molendi, Maccacaro & Schaeidt (1993) showed that Markarian 766 varied by a factor of ~ 3 in the two days of observation during the *ROSAT* all sky survey. Molendi & Maccacaro (1994) and Netzer, Turner & George (1994) used pointed *ROSAT* observations and concluded that the variable X–ray spectrum is not the result of a variable warm absorber. Markarian 766 has recently been observed with *ASCA* (Leighly et al. 1996), and was shown to have a warm absorber (evidenced by absorption edges at $\sim 0.7 - 0.8$ keV) and a variable power law component. Although a soft excess was detected, it is poorly constrained because *ASCA* is not sensitive to photons with energies < 0.4 keV.

1.3 The Structure of this Paper

The 9 *ROSAT* observations and details of the data reduction are presented in Section 2. The *ROSAT* data are examined in two ways: using data from three broad X–ray bands and spectral fitting at full resolution. Together they provide the maximum information about the spectral variability of Markarian 766 via the following procedure:

First, X–ray lightcurves are constructed in three energy bands (Section 3). Using the lightcurves as a guide, X–ray spectra are then constructed at six different flux levels (Section 4), allowing us to examine the spectral shape of Markarian 766 as it changes in brightness, and determine the contributions of the different emission components to the three X–ray bands. Variations in the three colour lightcurves and hardness ratios are then used to study variability of the emission components (Section 5) in a relatively model independent fashion. Finally, we cross correlate the flux in the three different bands to look for temporal relations between the emission at different energies (Section 6).

Our results are discussed in Section 7, and the X–ray and multiwavelength properties of Markarian 766 are compared to those of other NLS1s in Section 9. Our conclusions are presented in Section 10. We discuss the effect of the PSPC gain drift on the Markarian 766 data in Appendix A.

2 OBSERVATIONS

Details of the 9 *ROSAT* datasets used in this analysis are given in Table 1. We will refer to them as P1, P2, etc. All data were are REV2 data obtained using PSPC-B. All data were processed with the FTOOLS PCPICOR calibration task; all subsequent data reduction has been carried out using the Starlink ASTERIX package. The observations have been filtered using the same event rate and master-veto rate criteria, and all times with poor aspect solution have been excluded.

Markarian 766 was at the centre of the PSPC field of view during 4 of the observations. In the remaining 5 it was at different off-axis angles, ranging between 13.5 and 43.9 arc minutes (see Table 1).

Table 1. The 9 *ROSAT* observation datasets used in this analysis

Name	ROR number	start date	start MJD	observation length (seconds)	exposure time (seconds)	off-axis angle (arcmin)	count rate counts/s
P1	RP700221n00	15 June 1991	48422.0	86246	8313	19.4 *	1.1
P2	RP701203n00	16 June 1992	48789.2	426470	6563	0.0	3.8
P3	RP701056n00	18 June 1992	48791.1	419862	7178	43.9 *	2.2
P4	RP701091n00	8 Dec. 1992	48964.6	138240	5871	0.0	3.5
P5	RP701203m01	9 Dec. 1992	48965.1	8640	2597	39.6	3.8
P6	RP700970n00	21 Dec. 1992	48977.7	149472	14613	13.5	3.3
P7	RP701413n00	16 Dec. 1993	49337.5	25920	3093	39.0	3.1
P8	RP701353n00	17 Dec. 1993	49338.9	17280	3044	0.0	2.3
P9	RP701091a01	5 June 1994	49508.8	7600	2703	0.0	6.3

* In these observations Markarian 766 is close to the PSPC ribs

2.1 Comparing data from different observations

Comparison of data from the different *ROSAT* observations should only be made with considerable caution for two reasons:

1) The point spread function (PSF) changes with different off-axis angles.

2) The PSPC gain varies with off-axis angle and with time.

The PSF dependence on off-axis angle is reasonably well understood and is dealt with in Section 3.1.

The PSPC gain variation with time and off-axis angle, is well documented (Prieto, Hasinger & Snowden 1994, Snowden et al. 1995, Turner 1993) and its main effect is that on-axis spectra taken in the later stages of the PSPC-B lifetime are systematically different to spectra taken off-axis and/or earlier in the mission. This gain variation has some impact on this work, because it means that there is a significant difference in PSPC response between observations (P4, P8, P9) and the other observations. The FTOOLS task PCPICOR uses Al Kα detector gain maps, interpolated in time, to correct for the PSPC gain variations, and this has been applied to all the *ROSAT* data used here. This makes a significant improvement to the data but the authors consider that there are still some differences in response between the different observations; this is discussed in detail in Appendix A. However, the actual magnitude of the gain drift ($\sim$ 3% in the energy scale, before correction by PCPICOR, Snowden et al. 1995) means that it should have a very small effect on the colour based hardness ratios used in this work. Note that as well as the drift of the PSPC gain there was an intentional change of PSPC gain made in October 1991.

2.2 Use of Off-Axis Observations

The point spread function (PSF) of the *ROSAT* PSPC changes dramatically with off-axis angle, hence for the six different detector locations, different regions have been used for collecting source and background counts. Source and background regions were chosen to be at similar off-axis angles; they do not overlap with the region obscured by the PSPC rib support structure, and contain no contaminating bright sources. The use of observations with different off-axis angles is justified because the dependence of the *ROSAT* PSF with off-axis angle is well known except for the very low energy response (Hasinger et al. 1994a). In observations in which Markarian 766 is far off-axis (P3, P5 and P7), large circles (6 arc min radius) have been used as source and background regions to ensure that the majority of the source counts are included.

In two observations (P1 and P3), Markarian 766 was occulted by the ribs of the PSPC. To avoid any systematic errors in the X–ray flux as a function of time, data from all times when the source extraction region entered the ribs have been excluded; in general this means that only a portion of the spacecraft wobble period has been included (*ROSAT* wobbles once every 400 seconds to prevent the detector window wire grid from systematically occulting sources). Note that this procedure is not expected to introduce significant spurious variability because we used the *same* part of each spacecraft wobble. The effectiveness of this technique was verified using time filtered images and lightcurves folded on the 400 second wobble period of *ROSAT*.

Because of the proximity of Markarian 766 to the ribs in P1 it was necessary to use a small circle of only 0.9 arc min radius to collect source counts, and hence the correction for counts falling outside this circle is much larger for P1 than that for the other observations (see Section 3.1). P1 also differs from the other observations in that it took place before the October 1991 change of the gain (and hence spectral response) of the *ROSAT* PSPC-B detector. P1 contains the most time intensive monitoring of Markarian 766, and during P1 Markarian 766 was particularly faint; for these reasons it is a particularly interesting observation and is retained despite the technical difficulties.

3 THE THREE X–RAY BANDS

The primary purpose for constructing a light curve in three different X–ray bands is to examine how the overall spectrum changes with time. The three bands are therefore required to have energy responses which are as independent as possible to prevent the smearing out of spectral changes when photons of the same energy contribute to the flux in more than one band. With a proportional counter such as the *ROSAT* PSPC, it is impossible to find three energy bands which are *completely* independent. We have chosen the bands R1L, R4, and R7 (channels 11-19, 52-69 and 132-201 respectively) from Snowden et al. (1994). They are centred at approximately 0.2, 0.7 and 1.7 keV respectively, and their energy responses overlap with effective areas $< 10\%$ of their peak. Note that with bands this narrow, a large number of PSPC channels (and hence a considerable number of source counts) are excluded; this is acceptable because Markarian 766 is a bright source.

3.1 Correction for the PSPC PSF

It was noted in Section 2.2 that the *ROSAT* PSPC PSF changes with off-axis angle; some fraction of the PSF lies outside the circular region used to collect source counts. It is therefore necessary to renormalize the count rates to the full PSF before data from observations with different off-axis angles can be compared. The PSF of the *ROSAT* PSPC depends on energy as well as position. At the energies corresponding to the R4 and R7 bands, the dependence of the PSF with off-axis angle is well understood, and is described by the analytic expressions given in Hasinger et al. (1994a); R4 and R7 count rates have therefore been renormalized using these expressions.

Hasinger et al. (1994a) do not provide a good description of the PSF at low energies (i.e. the R1L band) because of a problem known as ghost imaging, in which the positions of low pulse height events can be incorrectly determined by the PSPC (see Snowden et al. 1994). The counts in R1L have been corrected using a Gaussian fit to the observed R1L PSF in each observation. The 90% statistical error on this Gaussian fit translates to a 5% uncertainty in the corrected R1L flux of observation P1, which has the largest uncertainty because only a small circle is used to collect source counts (see Section 2.2). In the other observations the renormalization of R1L amounts to a change of less than 10%, and hence the uncertainty on the R1L flux from the PSF correction is not likely to be more than a few percent.

3.2 Hardness Ratio Definitions

Two hardness ratios have been used to examine spectral changes:

$$HR_{\rm soft} = \frac{R4 - R1L}{R4 + R1L}$$

$$HR_{\rm hard} = \frac{R7 - R4}{R7 + R4}$$

Both $HR_{\rm soft}$ and $HR_{\rm hard}$ increase as the spectrum becomes harder.

3.3 The X–ray Lightcurves

To obtain good signal to noise (typically >30), counts in each band have been binned to 5760 seconds (i.e. 1 *ROSAT* orbit).

The X–ray lightcurves in the three X–ray bands for the four years of observation are shown in the top three panels of Fig. 1; note that the x-axis is not continuous. Markarian 766 exhibits substantial variability ($>$ factor 2 in the R4 and R7 bands) during every observation, excepting observations P5 and P9, which lasted only a single *ROSAT* orbit each. Hardness ratios, computed from the three light curves are shown in the bottom two panels of Fig. 1. Hardness ratio changes, and therefore changes in the spectral shape, are seen during all observations (again except P5 and P9 which are too short for the variability to be addressed). The variability will be quantified later in Section 5.2 when the 3 colour and hardness ratio variability is looked at in more detail.

4 SPECTRAL MODELING

4.1 Splitting the observations

Before relating the lightcurves and hardness ratio changes to changes in specific components of the X–ray spectrum of Markarian 766, it is necessary to examine the spectrum itself, and obtain a good spectral model.

The variable hardness ratios shown in Fig. 1 show that the spectrum is changing within the observations. We have extracted several spectra from each observation, that correspond to different levels of brightness of Markarian 766, to explore the full dynamic range of spectral shapes.

Traditionally, the overall *ROSAT* count rate would be used to define the intensity of the source (e.g. Molendi and Maccacaro 1994). This is not practical for the current dataset which includes observations at different off-axis angles because the broadband *ROSAT* count rate is sensitive to the position of the source on the PSPC. It must be convolved with a model spectrum to correct for the proportion of the PSF outside the source extraction circle, because the PSF is energy dependent. To extract spectra as a function of overall *ROSAT* count rate, consistently for each observation, would therefore require a prior knowledge of the spectra to be extracted.

This problem has been avoided by using the R4 count rate to define the intensity of Markarian 766, instead of the broadband count rate. R4 covers a narrow enough energy range that it is easy to correct for the PSF in a consistent way for all observations without a detailed prior knowledge of the spectrum. R7 could equally have been used; R4 has been preferred because it is more central in the *ROSAT* bandpass.

Six different levels of intensity have been defined according to the R4 count rate, and observations have been split up by their R4 count rates averaged in 5760 second bins, as shown in Table 2. For each observation, all counts collected during a given range of R4 count rate were combined to make a single spectrum. Up to six spectra were therefore constructed from each observation; as seen in Table 2 a total of 31 spectra were constructed.

We did not combine spectra from different observations because of their different off-axis angles and hence effective areas, and because of the possible response differences between the observations caused by the PSPC temporal/spatial gain drift. The effective area (as a function of energy) for each spectrum has been normalized to the source count collecting region using the analytical PSF expressions of Hasinger et al. (1994a).

Spectra were binned in energy with a minimum of 30 counts per bin, and analyzed using the spectral fitting program XSPEC; bad channels (1-7 and $>$ 200 for P1, 1-11 and $>$ 200 for the other observations, as defined in Snowden et al. 1994) were ignored and an additional sys-

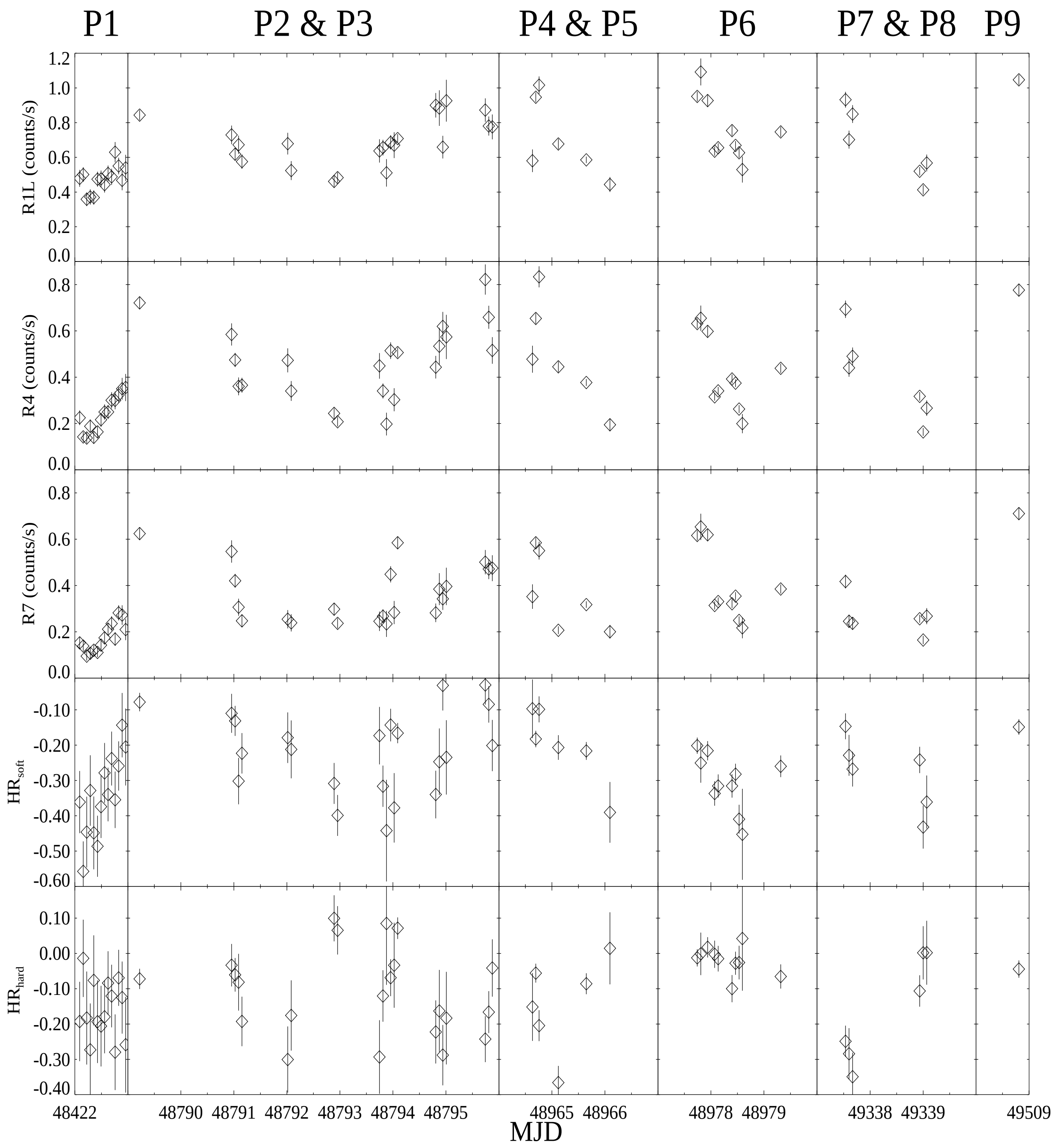

Figure 1. Variations in the 3 colour count rates and hardness ratios of Markarian 766 binned in *ROSAT* orbits (5760s). The vertical divisions indicate breaks between observations; the X–axis has the same scale for all observations.

tematic error of 2% assumed for each channel to reflect the uncertainty in the PSPC energy response. As stated above, observation P1 was made before the PSPC gain reduction in October 1991 and hence the spectra from this observation have been fitted using the high gain response matrix; the other observations have been fitted using the low gain response matrix. The 31 binned PSPC spectra are shown in Fig. 2.

4.2 Model Fitting

As a starting point for spectral modeling, we used a simple power law model with neutral absorption fixed at the Galactic column of 1.76×10^{20} cm^{-2} (Stark et al. 1992). The power law slope and normalization are fit individually for all 31 spectra. The fitted photon indices Γ range between 2.1 and 2.7 but the overall fit is very poor ($\chi^2/\nu = 1.9$ for 2261 degrees of freedom), and the residuals show evidence for both a soft excess and additional neutral absorption (see Fig. 4).

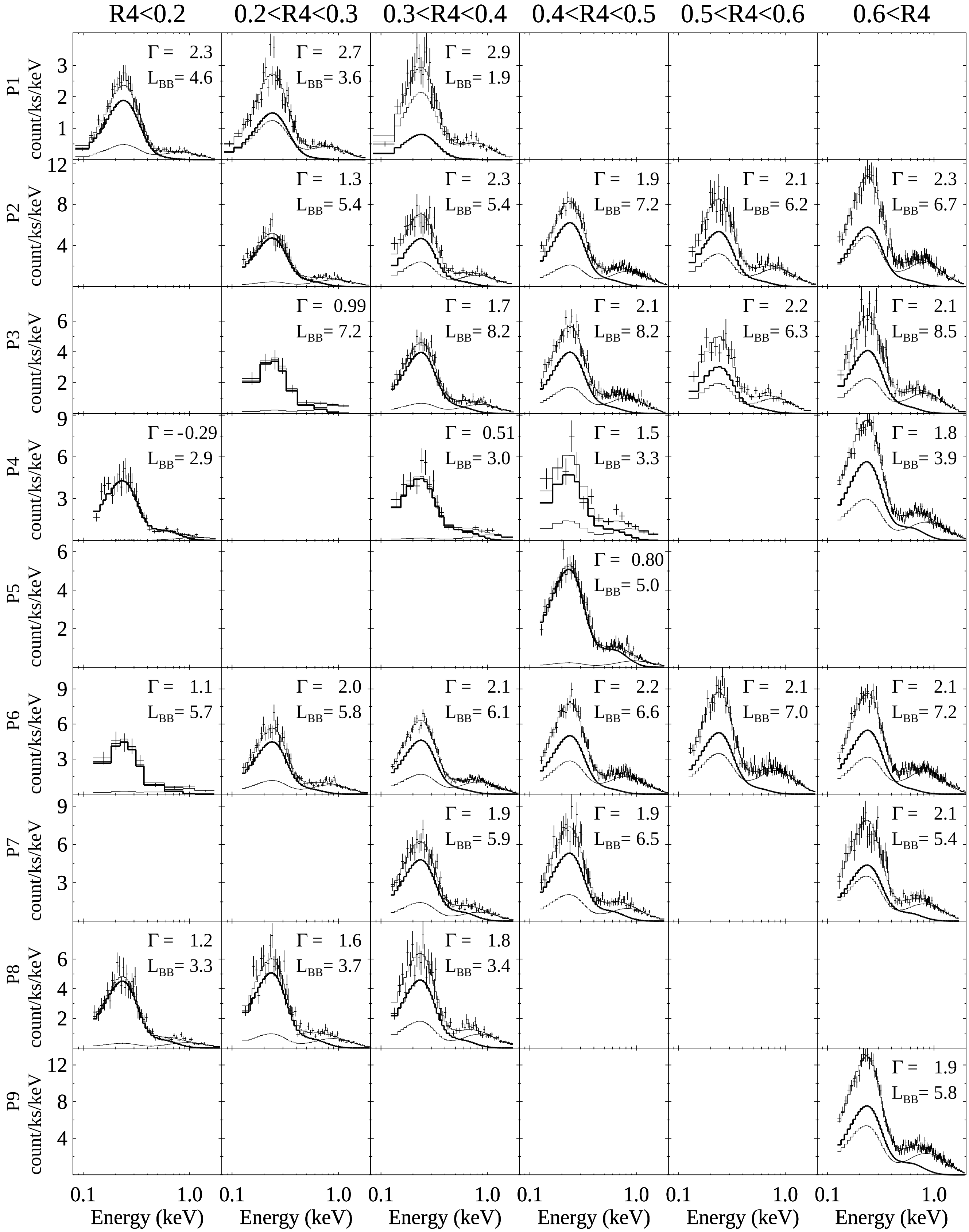

Figure 2. The 31 binned PSPC spectra (data points) with the best fitting power law + black body soft excess models as stepped lines: the power law and soft excess components are shown separately with the soft excess in bold, as well as the combined model. Γ is the photon index of the power law and L_{BB} is the normalization of the black body soft excess in units of 10^{37}ergs$^{-1}/D^2$ where D is distance to source in kpc. The remaining model parameters are given in row B of Table 3.

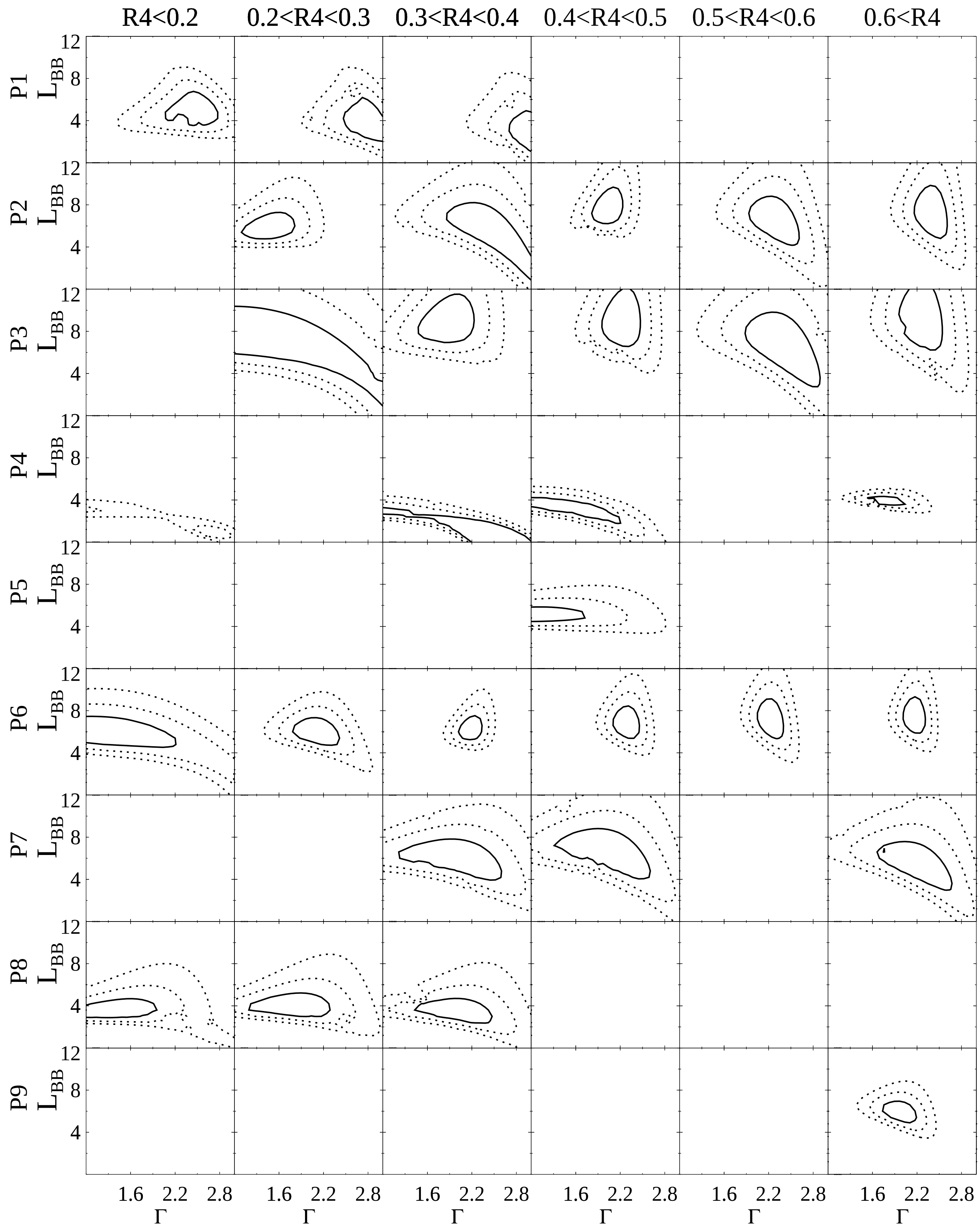

Figure 3. Confidence contours for the power law photon index Γ and black body soft excess normalization L_{BB} (in units of 10^{37}ergs$^{-1}/D^2$ where D is distance to source in kpc). The model is the same as the one used for Fig. 2 and the remaining model parameters are given in row B of Table 3.

Table 2. Exposure times of spectra taken for different R4 count rates and observations.

Data	time $R4 < 0.2$ (seconds)	time $0.2 < R4 < 0.3$ (seconds)	time $0.3 < R4 < 0.4$ (seconds)	time $0.4 < R4 < 0.5$ (seconds)	time $0.5 < R4 < 0.6$ (seconds)	time $0.6 < R4$ (seconds)
P1	4132	2803	1378	–	–	–
P2	–	1303	543	2856	575	1286
P3	–	216	2466	2874	571	1051
P4	870	–	343	189	–	4469
P5	–	–	–	2597	–	–
P6	165	1315	6683	2585	1502	2363
P7	–	–	1233	896	–	964
P8	1186	1047	811	–	–	–
P9	–	–	–	–	–	2703

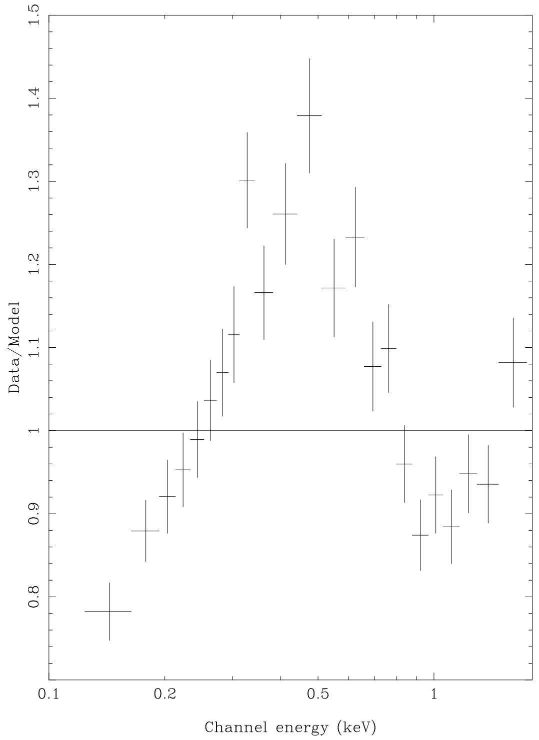

Figure 4. Ratio of the 0.4<R4<0.5 P2 spectrum to a power law model (best fit $\Gamma = 2.2$) with fixed Galactic $N_{\rm H}$. Note the residuals at the very lowest energies which are indicative of intrinsic neutral absorption and the bump from 0.3 to 0.7 keV which suggests a soft excess. For clarity the residuals are shown with larger energy bins than those used in the spectral fitting.

Allowing the absorbing column to vary in each spectral fit results in a significant improvement in the fit ($\chi^2/\nu = 1.3$ for 2313 degrees of freedom) and results in a mean column which is larger than the Galactic value. The redshift of Markarian 766 is low enough ($z = 0.013$), that using a redshifted absorber to represent the additional column instead of $z = 0$ column makes no appreciable difference to the goodness of fit or the fitted column; this was verified using XSPEC.

Addition of a blackbody component to represent the soft excess also results in a significantly better, although still poor, fit ($\chi^2/\nu = 1.2$ for 2199 degrees of freedom) with fixed $N_{\rm H}$. Adding a blackbody component *and* allowing the column to vary between spectra results in a good fit, with $\chi^2/\nu = 1.0$ for 2168 degrees of freedom.

A warm (partially ionized) absorber can often mimic the effect of a soft excess in *ROSAT* spectra. Its principal signature in the *ROSAT* band is the presence of absorption edges at 0.74 keV and 0.87 keV (rest energies) from O VII and O VIII respectively. These edges can not be resolved from each other with the *ROSAT* PSPC, and can be approximated as a single edge. It is known that Markarian 766 has a warm absorber from *ASCA* data. Approximating the warm absorber as a single edge in the *ASCA* data resulted in an observed edge energy of 0.75 keV (Leighly et al. 1996), and to keep the number of fitted parameters to a minimum we have used an edge with a fixed observed energy of 0.75 keV to represent a warm absorber. Substituting the blackbody soft excess with an edge at 0.75 keV, again leaving the neutral column free, results in $\chi^2/\nu = 1.1$ for 2199 degrees of freedom. This is better than the fit without the edge, but is much poorer than the fit with a soft excess (the edge model can be statistically rejected with 95% confidence). Including both an edge and a blackbody soft excess results in only a very slightly better χ^2/ν than using just the blackbody soft excess; an F-test shows that the improvement in the fit is not significant, hence we do not include an edge in our spectral models for the remainder of this paper.

A good fit to the *ROSAT* spectrum of Markarian 766 therefore requires three components: a power law, a soft excess and some intrinsic neutral absorption.

4.3 Absorption

In the previous section the neutral absorbing column was allowed to vary freely between spectra. The short term stability of this fitted column was tested by fitting the 31 spectra with only a single value of $N_{\rm H}$ for each observation (i.e. 9 values of $N_{\rm H}$), once using a blackbody, once using two black bodies with fixed temperatures of 50 eV and 80 eV (see Section 4.4), and once using a bremsstrahlung to represent the soft excess. χ^2 and fitted values of $N_{\rm H}$ are shown in Table 3; in each case a small reduction in χ^2/ν is found, compared to that when the column is fitted individually for each spectrum. The F-test shows that for any of these soft excess shapes, allowing $N_{\rm H}$ to vary within each observation does not lead to a significantly

Table 3. Fitting of spectra grouped by observation. For each model, χ^2/ν is given by observation and in total. In cases where spectra have been fitted using only a single value of one or more parameter per observation, the parameters are listed in parentheses beneath the model and values are given for each observation. Errors are 68% for one interesting parameter.

	Model	P1	P2	P3	P4	P5	P6	P7	P8	P9	Total
	Data points	175	417	305	225	84	612	194	158	153	2323
A	**BB**	166/162	353/396	298/284	253/208	86/79	596/587	162/181	187/145	134/147	2235/2190
	($N_{\rm H}$)	2.7±0.4	3.2±0.3	3.6±0.3	1.9±0.2	2.1±0.4	3.5±0.3	2.6±0.4	2.3±0.3	2.5±0.3	
B	**BB**	171/164	374/400	308/288	285/211	86/79	609/592	164/183	198/147	134/148	2329/2212
	(T)	54±5	68±4	69±5	91±5	96±6	65±5	82±7	77±5	88±5	
	($N_{\rm H}$)	3.0±0.4	3.7±0.3	3.7±0.4	2.1±0.3	2.1±0.4	3.7±0.3	2.8±0.3	2.7±0.4	2.5±0.3	
C	**BR**	186/162	360/396	307/284	252/208	79/79	589/587	170/181	181/145	139/148	2254/2190
	($N_{\rm H}$)	3.1±0.2	3.7±0.4	3.9±0.4	2.9±0.1	3.1±0.2	4.0±0.2	3.2±0.3	3.0±0.1	3.0±0.2	
D	**2BB**	163/162	350/396	297/284	276/208	93/79	586/587	164/181	188/145	138/148	2255/2190
	($N_{\rm H}$)	3.1±0.2	3.7±0.4	3.9±0.4	2.9±0.1	3.1±0.2	4.0±0.2	3.2±0.3	3.0±0.1	3.0±0.2	

BB model spectrum has a power law, a blackbody soft excess and absorption by neutral material
2BB model spectrum has a power law, two black bodies at temperatures of 50 eV and 80 eV to represent the soft excess, and absorption by neutral material
BR model spectrum has a power law, a bremsstrahlung soft excess and absorption by neutral material
T is the blackbody temperature in eV
L_{BB} is the blackbody normalization in units of $10^{37}\,{\rm ergs}^{-1}/D^2$ where D is distance to source in kpc
$N_{\rm H}$ is the neutral absorbing column in units of $10^{20}{\rm cm}^{-2}$

better fit than using a single value of $N_{\rm H}$ for each observation, and when the column is allowed a different value for each spectrum within an observation, consistent values are found. This shows that there is no detectable change in the fitted neutral absorbing column within any of our observations, regardless of which model is used for the soft excess. The different fitted column values from the different observations could be caused by the temporal/spatial gain variation of the PSPC; see appendix A for some discussion of this.

4.4 The Shape of the Soft Excess

Several models were tried for the soft excess component, and the lowest χ^2 was found for a single blackbody (model A in Table 3). The soft excess was also parameterized as a bremsstrahlung and as two black bodies (with energies fixed at 50 and 80 eV), both of which have broader shapes than a single black body. The values of χ^2 are slightly poorer for these models (C and D in Table 3) but they are still acceptable fits to the data, with $\chi^2/\nu = 1.0$.

4.5 Variability of the model components

It is obvious from the variable R4 and R7 count rates, that the power law component is variable in amplitude. To investigate variability of the power law slope and the soft excess, we assumed a black body shape for the soft excess (this has the lowest χ^2 of the three shapes tried) and fitted the spectra with a single soft excess temperature for each observation. The χ^2, fitted columns and fitted temperatures are given in Table 3, model B. This model is an acceptable fit to the data at the 95% confidence level. The models and data are shown in Fig. 2 and each spectrum is labeled with the best fit power law slope and black body luminosity. Confidence contours for these two fitted parameters are shown in Fig. 3. In each observation, a single value of the black body luminosity can be found that is consistent with all the different count rate spectra, i.e. there is no detectable change of soft excess flux within any of the observations. However, there is a trend for harder power laws at lower R4 count rates. This trend is more obvious when the power law slope and normalization are plotted in Fig. 5. The trend for harder slopes at low normalization is seen when the different observations are compared *as well as* in the individual observations. The three outlying points to the top left of Fig. 5 are all from observation P1, and the difference between the power law parameters from this observation and the others is likely due to the much smaller source circle in P1 and the different gain state of the PSPC; note that the trend for harder power laws at lower normalization is still present within the P1 observation itself.

4.6 Overall Characterization of the Markarian 766 PSPC Spectrum

The spectral fitting described above shows that:

1) The PSPC spectra can be adequately described with a power law component, a soft excess component, and a neutral absorbing column.
2) There is no evidence that the neutral absorbing column changes within any observation.
3) The soft excess component is well characterized by a black body shape peaking at < 0.3 keV.
4) Variability of the soft excess component is not detected.

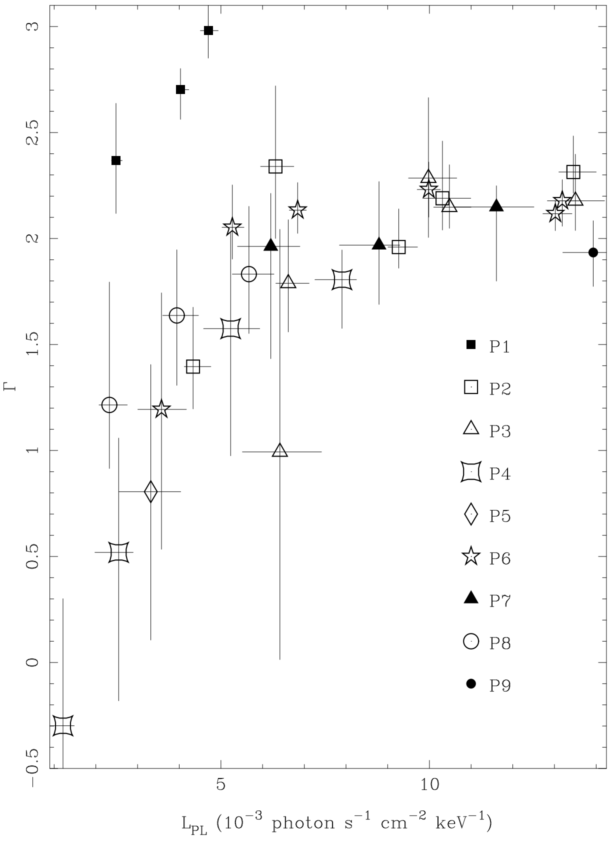

Figure 5. Behaviour of the power law component when the soft excess is modeled with a blackbody shape.

5) The power law component becomes harder when it becomes fainter.

However, points 4) and 5) in particular are somewhat model dependent in that the spectral fitting process depends on the exact shape of the soft excess (which is not known) and in that the different model components are strongly correlated with each other in the fitting. The three X–ray bands R1L, R4 and R7 will be used in the next section to investigate the spectral variability of Markarian 766 in a way that is *not* strongly model dependent.

5 THREE COLOUR AND HARDNESS RATIO VARIABILITY

We now return to the lightcurve and hardness ratios shown in Section 3. In light of the spectral modeling results presented in the previous section, the variability in the three X–ray bands R1L, R4 and R7 is examined and related to variability of the power law and soft excess components. Each observation will be examined separately to ensure that the results are robust against the different positions that Markarian 766 has on the PSPC in different observations, and to ensure that the temporal/spatial uncertainty in the PSPC gain has a minimal effect. Variability in observations P5 and P9 can not be examined in detail because they were only a single *ROSAT* orbit (5760 seconds) in duration.

The count rates in the three X–ray bands are strongly correlated with each other, both between and within the observations, as shown in Fig. 6. When data from all the observations are combined, the probability that any of the pairs of bands are not linearly correlated is $< 10^{-18}$; the dashed lines in Fig. 6 are the best fitting straight lines to the (R4,R1L), (R7,R1L), and (R7,R4) relations, and comparison with data from individual observations reveals that the source always varies in a similar fashion. Treating the dashed lines as crude estimates of the (R4,R1L), (R7,R1L), and (R7,R4) relations, it is seen that when R7=0 (i.e. the power law component has disappeared) there is still considerable flux (~ 0.2 counts/s) in the R1L band. The same is true when R4=0, but the dashed line for (R7,R4) passes closer to (0,0). This 'residual' flux in R1L betrays the presence of the soft excess, and confirms that it peaks in the R1L band.

5.1 Changes in the Spectrum

The variability can be examined in more detail by comparing hardness ratios with count rates in the three bands, and allows questions to be asked such as whether the change in power law flux is accompanied by a change in power law slope, and whether variability of the soft excess, as well as variability of the power law, is required by the data. The most robust comparisons are between HR_{hard} and R1L, and between HR_{soft} and R7. R1L is not used in the calculation of HR_{hard}, hence the errors on the two quantities are independent; similarly for R7 and HR_{soft}. We will examine changes in hardness ratios within the five longest observations: P1, P2, P3, P4 and P6; the other observations have too few data points to examine hardness ratio changes properly.

These hardness ratios will be compared to models of how they should behave as the different components vary. We will describe the soft excess using the parameters appropriate for a black body absorbed by a neutral column of $3 \times 10^{20}\mathrm{cm}^{-2}$. However, the detailed shape of the soft excess does not matter for the three colour study because the soft excess is only observed in the two bands R1L and R4: any change in shape of the soft excess has the same effect as changing the black body temperature, i.e. it changes the contribution of the soft excess to R4 relative to R1L.

From the spectral modeling performed in Section 4, one can estimate the extent of parameter space which requires investigation. Table 3 shows that when the soft excess is described as a blackbody, most data are consistent with a temperature T between 60 eV and 80 eV. The maximum fitted temperature of 96 eV, and a blackbody component at this temperature or less has an R7 count rate which is at least 45 times smaller than the R1L and R4 count rates, even when attenuated by a neutral absorbing column of $3 \times 10^{20}\mathrm{cm}^{-2}$. Similarly, when the soft excess is modeled as two black bodies, the contribution to R7 is negligible. Even when the soft excess is modeled using the much broader bremsstrahlung shape, the highest fitted bremsstrahlung temperature ($\sim$0.2 keV) leads to an R7 count rate which is 15 times smaller than the R1L or R4 count rates. We can therefore assume that the soft excess, whatever its shape, provides a negligible contribution to the R7 count rate.

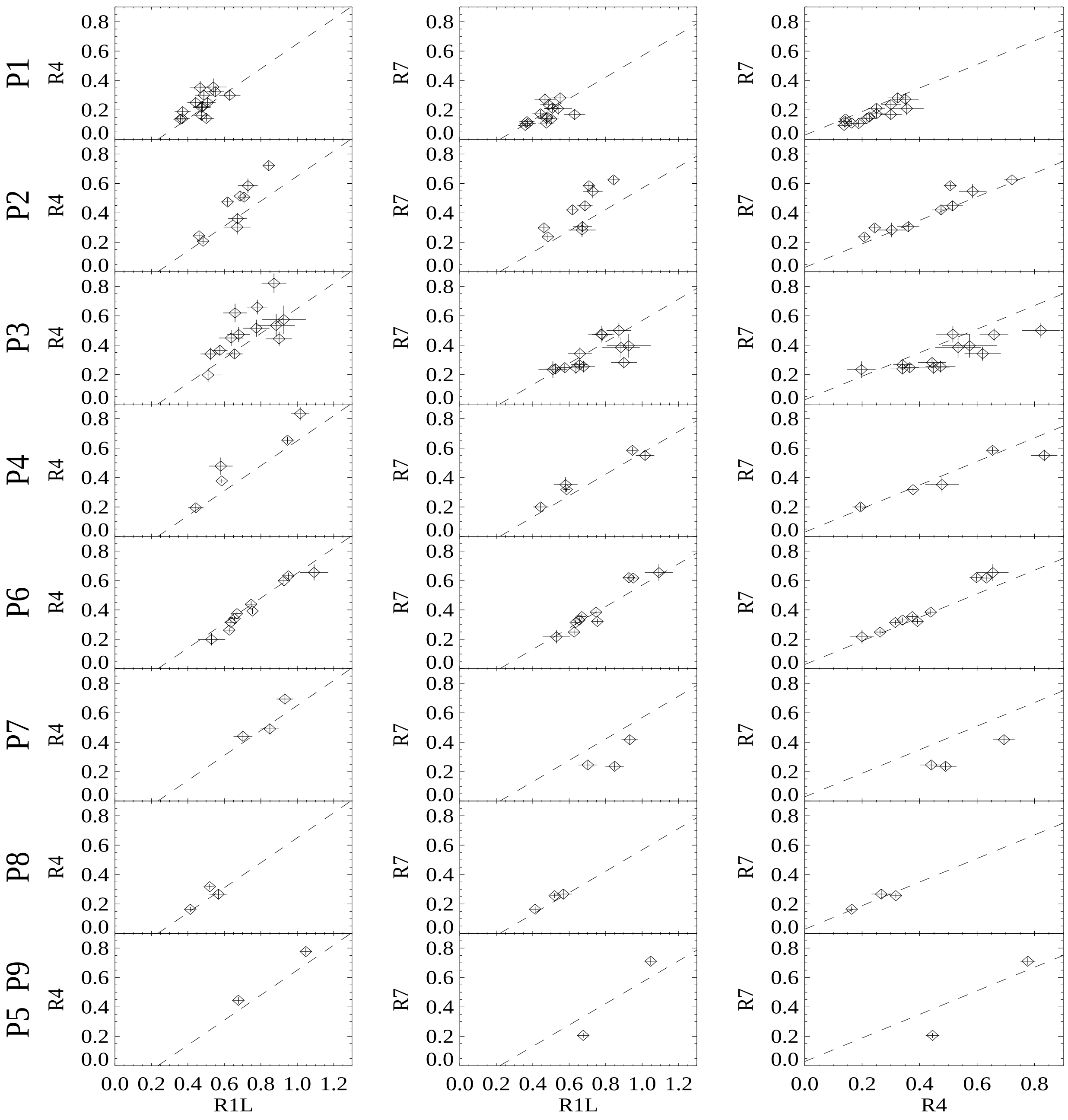

Figure 6. Comparison of the count rates for Markarian 766 in the 3 X–ray bands R1L, R4 and R7. Each observation is shown separately, except P5 and P9 which are shown together. The same dashed lines are plotted for each observation, and represent linear fits to the combined 3 colour data from all the observations.

Fig. 3 shows that the black body soft excess normalization L_{BB} lies between 3 and 9 ($\times 10^{37}$erg s$^{-1}/D^2$, where D is the distance to Markarian 766 in kpc), and the majority of fitted power law slopes have $1.7 < \Gamma < 2.3$.

The hardness ratios are plotted in Fig. 7 and repeated in Figs. 8 and 9. Each solid curve is the expected locus of hardness ratios for pure flux variability (i.e. no change in slope) of the power law component, with a constant soft excess; curves are provided for a range of soft excess temperatures in Fig. 7, soft excess normalizations in Fig. 8 and power law slopes in Fig. 9. Note that we have made no attempt to 'fit' the data in this section.

The relation between HR_{soft} and the R7 count rate can be reproduced well by pure flux variability of the power law. For any combination of soft excess parameters and power law slopes, power law flux variability predicts that HR_{soft} should increase with R7, which is the observed behaviour.

However, pure flux variability of the power law predicts that HR_{hard} is a monotonically increasing function

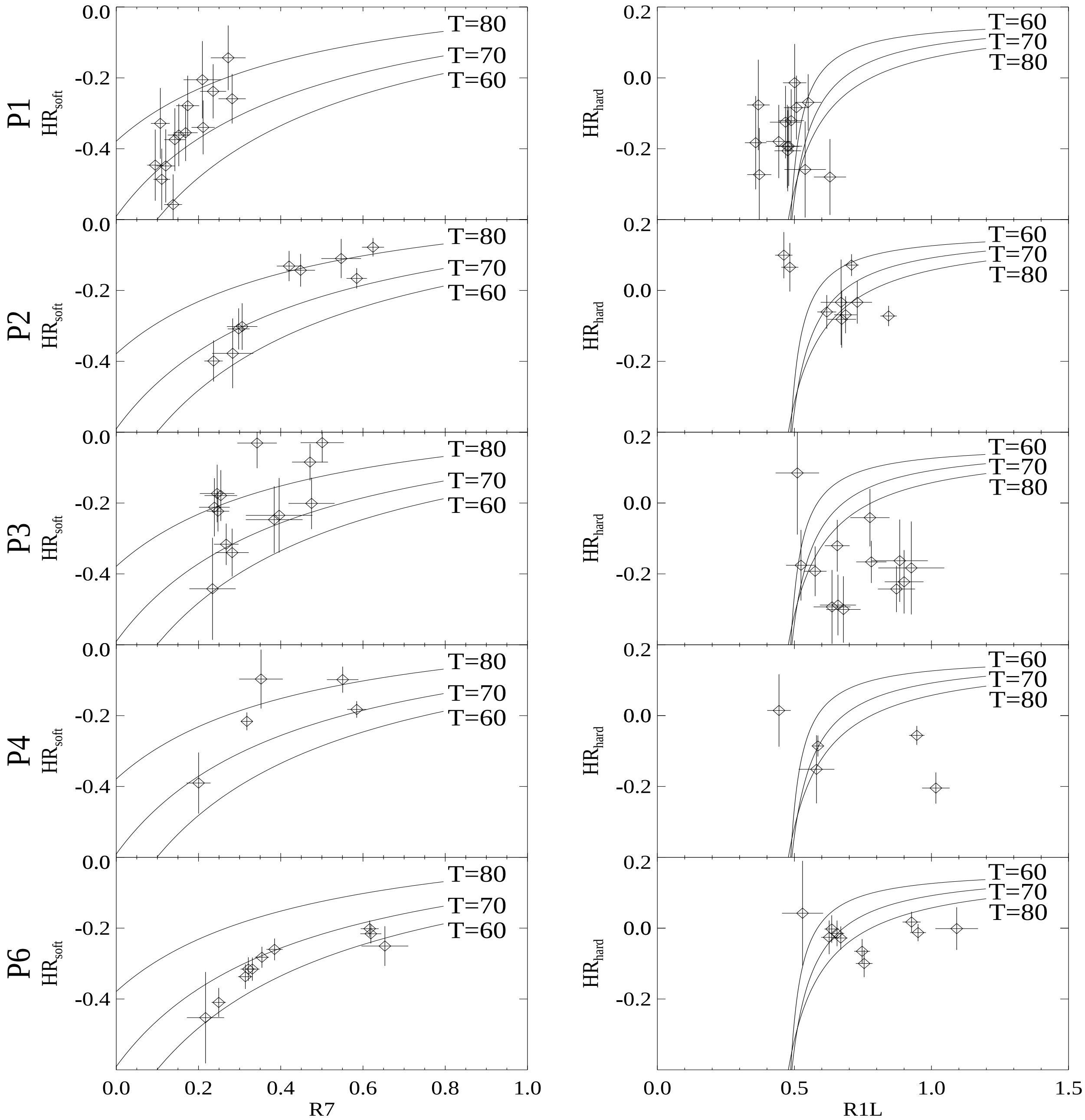

Figure 7. HR_{soft} as a function of (hard) R7 count rate and HR_{hard} as a function of (soft) R1L count rate. The model curves are for flux variability of a $\alpha = 1$ power law; the soft excess has normalization $L_{BB} = 6 \times 10^{37}$ergs$^{-1}/D^2$ (where D is the distance in kpc), and temperature T in eV as indicated on the curves.

of R1L count rate. This does not match the observed behaviour of HR_{hard}, which *does not* increase with R1L for R1L < 0.8 as seen in Figs 7 to 9. The relation between HR_{hard} and R1L can be reproduced by a steepening of the power law with increasing power law flux (see Fig. 9) and/or an increase in the soft excess normalization (see Fig. 8) with increasing power law flux. In the latter case, to reproduce the variability of HR_{hard}, the soft excess must vary by a factor of ~ 3, and since the higher soft excess normalization is required at higher R4 count rates its variability must be correlated with that of the power law component.

5.2 Variability Amplitude

A simple means of examining the variability of the different spectral components is to compare the variability amplitude in the three X-ray bands. For this we have used the normalized variability amplitude, which is defined as the standard deviation σ_{int} divided by the mean count

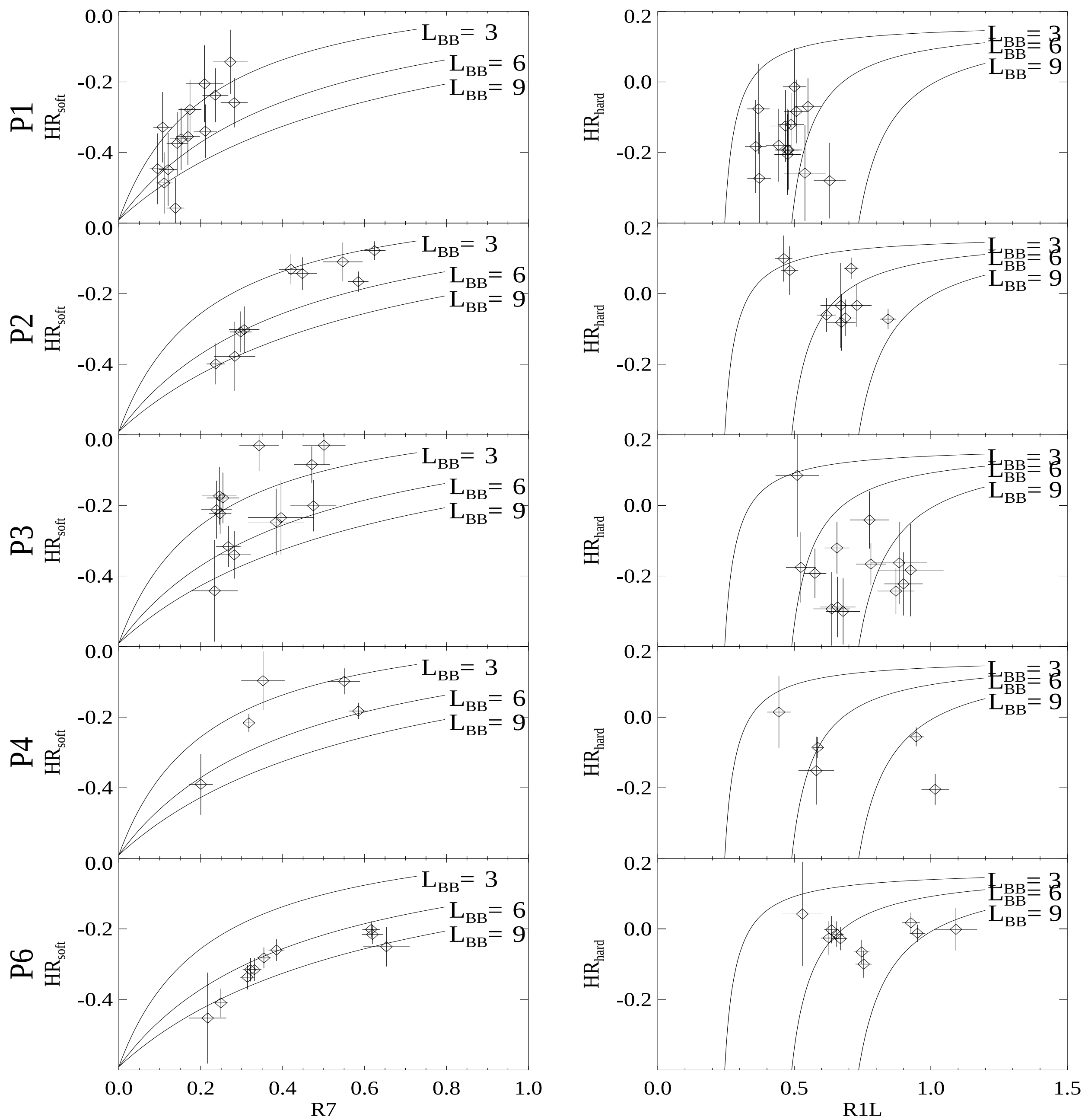

Figure 8. HR_{soft} as a function of (hard) R7 count rate and HR_{hard} as a function of (soft) R1L count rate. The model curves are for flux variability of a $\alpha = 1$ power law; the soft excess has a temperature of 70 eV and normalization L_{BB} (in units of 10^{37}ergs$^{-1}/D^2$ where D is the distance in kpc), as indicated on the curves.

rate. This is corrected for measurement errors by assuming that

$$\sigma_{int}^2 = \sigma_{obs}^2 - \sigma_{err}^2 \quad (1)$$

where σ_{int} is the true standard deviation, σ_{obs} is the observed standard deviation, and σ_{err} is the measurement error (see Edelson 1992).

The variability amplitude in the three bands is shown in Table 4. The 1σ error quoted is calculated from equation 2 in Done et al. (1992a) and is the uncertainty in the width of an assumed underlying Gaussian distribution of count rates from which the data were drawn; note that this is not the measurement error of the count rate, which has already been subtracted in quadrature (Eq. 1). In *every* observation the variability is smaller in the R1L band than in either R4 or R7. This shows that the more variable component is the power law, which dominates the flux in R4 and R7 bands. The reduced variability amplitude in R1L shows that the soft excess is relatively invariant, diluting the overall (power law + soft excess) R1L

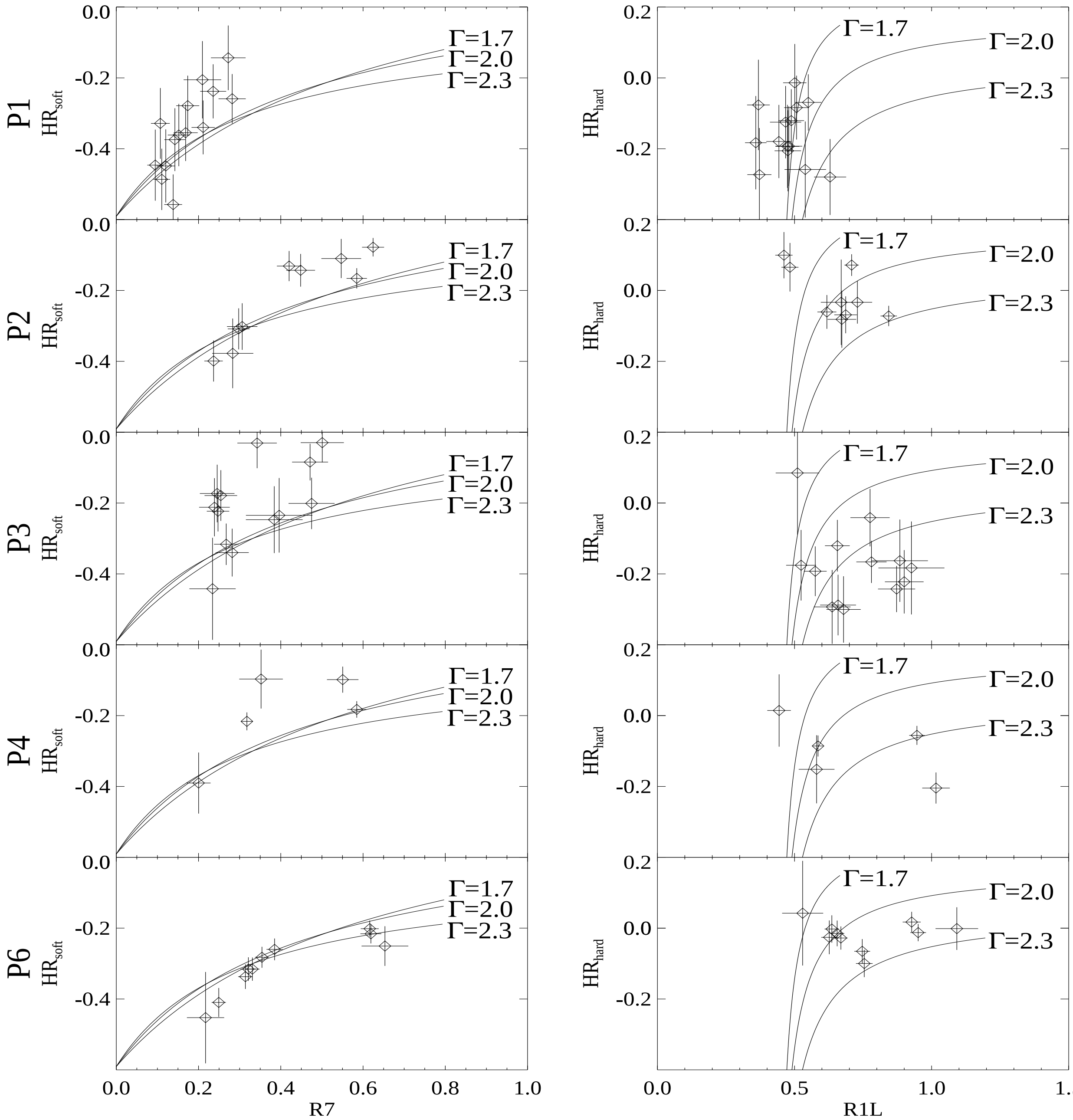

Figure 9. HR_{soft} as a function of (hard) R7 count rate and HR_{hard} as a function of (soft) R1L count rate. The model curves are for flux variability of power laws with slopes $\alpha = 0.7$, $\alpha = 1.0$ and $\alpha = 1.3$. The soft excess has temperature $T = 70$ eV and normalization $L_{BB} = 6 \times 10^{37} erg s^{-1}/D^2$ (where D is the distance in kpc).

variability. This means that to explain the hardness ratio variability in Section 5.1, the power law slope *must* vary.

6 CROSS CORRELATION ANALYSIS

The time dependence of flux changes at different energies is potentially a powerful discriminator between different models for the emission mechanisms (see Section 1.1). It has been studied by cross correlating the count rates in the three bands using the discrete correlation function (DCF hereafter, see Edelson and Krolik 1988).

The DCF for the R1L and R4 lightcurves is defined as

$$\mathrm{DCF}(\tau) = \frac{1}{M} \sum \frac{(R1L(t) - \langle R1L \rangle)(R4(t+\tau) - \langle R4 \rangle)}{\sigma_{R1L} \quad \sigma_{R4}}$$

where the sum is made over all M values of t for which there is a measurement of R1L at time t and a measurement of R4 at time t+τ. $\langle R1L \rangle$ and $\langle R4 \rangle$ are the mean R1L and R4 count rates respectively; σ_{R1L} and σ_{R4} are the standard deviations of the R1L and R4 count rates re-

Table 4. Normalized variability amplitude in the three X–ray bands for each of the observations.

ROSAT pointing	number of points	R1L variability amplitude (%)	R4 variability amplitude (%)	R7 variability amplitude (%)
P1	14	12^{+4}_{-2}	32^{+10}_{-6}	31^{+10}_{-6}
P2	9	19^{+9}_{-4}	34^{+16}_{-7}	33^{+16}_{-7}
P3	13	17^{+6}_{-3}	29^{+10}_{-5}	29^{+10}_{-5}
P4	5	35^{+19}_{-12}	48^{+25}_{-16}	41^{+22}_{-14}
P6	10	20^{+9}_{-4}	38^{+16}_{-8}	40^{+17}_{-8}
P7	3	13^{+23}_{-4}	22^{+40}_{-7}	35^{+63}_{-11}
P8	3	9^{+16}_{-3}	32^{+58}_{-10}	19^{+34}_{-6}

spectively and have been corrected for measurement error using equation 1 in Section 5.2. The standard error on the DCF is defined as

$$\sigma_{DCF}(\tau) = \frac{1}{M-1} \times \tag{2}$$

$$\sqrt{\sum \left[\frac{(R1L(t) - \langle R1L\rangle)(R4(t+\tau) - \langle R4\rangle)}{\sigma_{R1L}\ \ \sigma_{R4}} - DCF(\tau)\right]^2}$$

The DCF is similarly defined for any combination of R1L, R4 and R7. This method is appropriate to our *ROSAT* data since it requires no interpolation, and provides simple error estimates.

ROSAT wobbles with a period of 400s, preventing the wire grid of the PSPC window from permanently masking sources; 400s is the smallest time binning which does not introduce spurious variability associated with the spacecraft wobble. Hence lightcurves with 400s time bins have been cross correlated. Due to the orbital interruptions in *ROSAT* observations the number of pairs available for cross correlation is very small for time differences greater than 1200 seconds. Only the five longest observations have been used: the others are too short to provide a useful number of pairs for cross correlation.

The results of the cross correlation analysis are shown in Fig. 10. The error bars are 68% as given by equation 2 above. The cross correlation was intended to reveal whether changes at the soft energies precede changes in the hard power law or vice-versa. The time bins are the same for all three bands, so there is no asymmetry in the DCF originating from the temporal sampling. Since the points of the DCF are not independent, we require some simple means of testing the significance of the observed DCF against the null hypothesis that neither component leads the other. We have used a bootstrap error method: for each time lag, pairs of points were chosen at random from all the original pairs with corresponding positive *or* negative time lag and the DCF constructed with the same number of pairs as the real DCF; this was repeated 1000 times and the solid line in Fig. 10 corresponds to the region bounding 68% of the symmetrical bootstrap simulations. It is seen in Fig. 10 that the only significant deviation from the symmetrical bootstrap simulations is in observation P1 where there is a marked asymmetry in the DCF of R1L and R4. To improve the signal to noise further, the DCF has been computed using a single bin for positive time lags and a single bin for negative time lags. Applying our bootstrap error method we find that the observed asymmetry of the DCF of R1L and R4 is just significant at the 95% level, and that of R1L and R7 is significant at 85% for observation P1. The DCF is within the 68% confidence limits for R7 and R4 in observation P1 and for all combinations of R1L, R4 and R7 for the other observations.

Thus, in P1, when Markarian 766 is at its faintest, and consequently the power law component is smallest relative to the soft excess, changes at < 0.5 keV appear to precede changes at > 0.5 keV. However, it must be pointed out that the cross correlation has been performed on 5 datasets, of which only one has 95% significant asymmetry; the probability of one or more dataset having this level of asymmetry, by statistical fluctuation alone, is 23%.

7 DISCUSSION

7.1 Long and Short Term Variability Properties of Markarian 766

There is no apparent long term variability trend present in the *ROSAT* observations of Markarian 766; changes in the *ROSAT* count rate between observations are no larger than the changes seen in individual observations. On a time scale of hours, Markarian 766 varies continuously in every observation period. The spectral variability takes the same form in every observation, which can be explained by variability of the power law slope and normalization.

Given that the behaviour is the same throughout the PSPC pointed observations from 1991 to 1994, the same spectral variability would be expected in the *ASCA* observation of Markarian 766 in 1993. Leighly et al. (1996) report that the major change in the *ASCA* band was that the power law slope became steeper as the power law flux in the *ASCA* band increased. This behaviour is entirely consistent with the spectral variability seen in the *ROSAT* observations and reported here. Similarly, in the *EXOSAT* ME observations of 1985 and 1986 steeper power law photon indices are found for increased power law normalization (Molendi, Maccacaro & Schaeidt 1993).

7.2 The Origin of the Power Law

There are two popular models for the power law X–ray component of radio quiet AGN; both are based on Compton upscattering of UV or soft X–ray photons from an

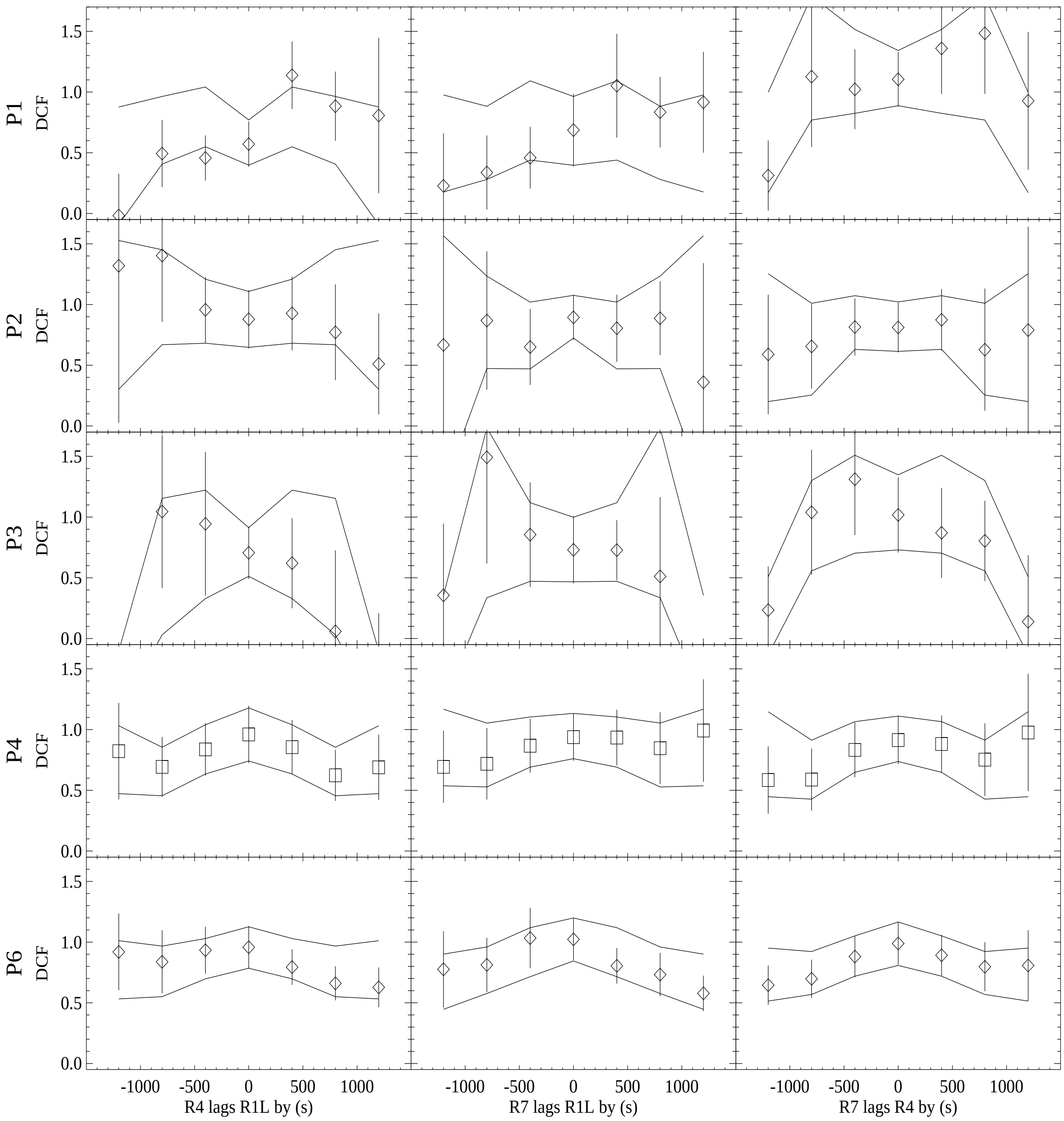

Figure 10. Discrete correlation function (DCF) of R1L, R4, and R7 for the five long observations. The solid lines are the bootstrap 68% confidence limits to the DCF if it is symmetric.

accretion disk or optically thin plasma. In the first model, the observed power law emission is simply that from upscattering of the soft photons in a hot (kT $\sim$ 500 keV) plasma, or by a non - thermal distribution of relativistic electrons (Walter & Courvoisier 1992). In the second model, the emission originates in a region in which the radiation density is large enough that the region is opaque to photon - photon collisions (γ–ray - γ–ray or γ–ray - X–ray) which give rise to electron - positron pairs. These pairs down scatter the γ–ray radiation and produce the observed X–ray spectrum, including the soft X–ray excess (Zdziarski et al. 1990). *Both* these models predict that in the variability of a single source the power law slope is softer when the power law flux is higher (Done & Fabian 1989, G. Torricelli-Ciamponi & Courvoisier 1995) as observed in Markarian 766.

Leighly et al. (1996) show that Markarian 766 has sufficient radiation density in the emission region that pair production may be important. The compactness parameter is defined as

$$l = L\sigma_T / R m_e c^3$$

where L is the luminosity, R is the size of the source, σ_T is the Thompson scattering cross section, m_e is the mass of the electron and c is the speed of light; pair production may be important if $l > 10$ (Svensson 1987). Using the shortest factor 2 variability time from the *ASCA* lightcurve ($\Delta t \sim 1000s$) to define the size of the source, assuming $R < c\Delta t$, Leighly et al. found $l \sim 12$. Leighly et al. (1996) propose that the variability observed during the *ASCA* observation is best explained by pair reprocessing, because the major spectral variability was confined to a single rapid increase in the flux of Markarian 766 (after which it remained relatively constant), and because the soft excess is not required to fit the high count rate spectrum. This would be expected if the energies of the relativistic electrons were to increase suddenly: the first order pair reprocessed spectrum (seen as the soft excess) is replaced by a non-linear pair cascade, which produces the $\alpha \sim 1$ power law spectrum.

However, from the *ROSAT* observations it is clear that the soft excess *does not* disappear when the power law increases in flux and slope, as this would lead to exactly the opposite behaviour of HR_{hard} from that seen in figs 7 to 9.

If the spectral changes in a source of compactness $l \sim 12$ are determined by pair reprocessing, the hard X–rays would be expected to vary $\sim$ half a light crossing time before the soft X–rays (Done & Fabian 1989). Assuming 1000s as the light crossing time for Markarian 766 this delay is $\sim$ 500s. This should lead to a significant asymmetry in the cross correlations in Fig. 10 such that changes in the R7 band (and to a lesser extent R4 band) lead the changes in the R1L band. No such asymmetry is seen (the DCF from observation P1 is asymmetric in the opposite sense).

If the power law component is produced by relativistic particles scattering soft photons and pairs are not important, then changes in the power law component may be simultaneous at all energies. If the variability of the power law component is driven by changes in the number of soft seed photons (i.e. variability of the soft excess) then this could explain the apparent asymmetry, with soft flux leading the hard flux, in the cross correlation of observation P1. However, in current models (e.g. Torricelli-Ciamponi & Courvoisier 1995), the change in spectral index with power law flux is brought about by a change in the relativistic electron energy spectrum, not a change in the number of soft photons, and hence there is no expectation that the soft flux should change first. This would explain how the power law varies when there is no detectable soft excess variability, and is consistent with the behaviour of $HR_{\rm hard}$ in all the observations.

7.3 The Origin of the Soft Excess

The low variability amplitude in the R1L band compared to the harder R4 and R7 bands (see Table 4) would suggest that the soft excess is relatively invariant on short time scales compared to the power law component. This suggests that the soft excess and power law are different components, and hence a pair reprocessing origin for the soft excess is not likely.

The relative invariance of the soft excess also rules out models whereby the soft excess is power law emission reflected or reprocessed close to the central regions. However, if the soft excess were power law emission reprocessed at regions some distance (light days or more) from the central regions, then the soft excess variability would be smeared out by the long response; such a model is therefore compatible with the *ROSAT* data.

The lack of short term soft excess variability is consistent with the it being part of the big blue bump, which is known to have a longer variability time scale than the power law X–ray emission in radio quiet AGN (e.g. NGC4051, Done et al. 1990). The soft excess spectrum is well fit by one or two black bodies, and hence is consistent with the shape expected from the high energy tail of a hot accretion disk (e.g. Ross, Fabian & Mineshige 1992.)

It is not possible to determine if the soft excess of Markarian 766 varies over a longer time scale than an observation; different values for the blackbody parameters are obtained from different observations, but the difference in off-axis angles between the observations, and the gain drift of the *ROSAT* PSPC, mean that long term soft excess variability cannot be assessed with any certainty.

We note that the results presented here, i.e. that short term variability in the soft excess component is not detected, are in marked contrast with the findings of Molendi & Maccacaro (1994). Their study of Markarian 766 is based on observation P2, in which they find that the soft excess varies with the power law component by approximately the same amplitude, and hence that the two components are related to the same physical process or are causally connected. However, they determine the blackbody and power law parameters by fitting models to spectra in four states defined by overall count rate. They do not quote uncertainties on the power law and blackbody normalizations; the apparent correlation between blackbody and power law normalization may be caused by the coupled nature of the blackbody temperature and power law slope when fitting low resolution *ROSAT* spectra. The three colour data (see Fig. 6), and lower variability amplitude in R1L than the R4 and R7 (Table 4), for all the *ROSAT* observations, including P2, show that the blackbody flux *can not* vary as much as the power law flux. Consequently, the model presented by Molendi & Maccacaro whereby changes in the accretion rate of an accretion disk determine the variability time scales in the *ROSAT* band is not valid, because the soft excess, assumed to be the high energy tail of an accretion disk, probably does not vary with the time scales found in the *ROSAT* lightcurve.

8 ANALOGY WITH GALACTIC BLACK HOLE CANDIDATES

Galactic black hole candidates (GBHCs) have X–ray spectra that are qualitatively similar (power law component with a soft excess, an Fe line and reflection hump), to those of Seyfert 1 galaxies. Both types of objects are thought to be powered by accretion onto a black hole, and it is possible that the physical processes which produce X–ray emission are the same in both types of objects. GBHCs have two states: in the 'low' state they have hard ($0.3 < \alpha < 0.8$) power law spectra with low energy

(< 2 keV) soft excesses and in the 'high' state they have steep power law components ($1.3 < \alpha < 1.8$) and powerful soft excesses which dominate the spectra below ~ 8 keV (Ebisawa et al. 1996). In the low state, GBHCs exhibit very rapid (millisecond) variability of the power law component, but vary less rapidly when they are in the high state.

The connection between GBHCs and Seyfert 1 galaxies has been strengthened by the discovery that RE J1034+396 has an extremely powerful soft excess, a steeper power law component than most Seyfert 1s, and does not vary rapidly, i.e. it is like a GBHC in a high state (Pounds, Done & Osborne 1995). In this analogy, Markarian 766 is equivalent to a low state GBHC in that it shows continuous variability of the power law component, the spectral index of which is similar to those found in low state GBHCs. The variability time scales of GBHCs are much smaller than those of Seyfert galaxies like Markarian 766, but this is not surprising given the large difference in the central black hole masses and hence overall dimensions inferred for Seyfert nuclei and GBHCs. It is believed that the soft excess in the GBHC Cygnus X-1 comes from a region of larger spatial extent (and hence varies on a longer time scale) than that producing the power law emission (Done et al. 1992b); the results presented here show that the same is probably true for Markarian 766. Furthermore, changes in the soft X-ray flux in Cygnus X-1 lead changes in the hard X–ray flux (Miyamoto & Kitamoto 1989), which may be true also for Markarian 766 in observation P1 (see Section 6).

Note that ultrasoft spectra (*ROSAT* $\Gamma > 3$) are not found in Seyfert 1s with broad lines (FWHM > 3000 km s^{-1}, Boller, Brandt and Fink 1996), i.e. the broad line Seyfert 1s are only analogous to GBHCs in the low state. However, *both* GBHC states are represented among the NLS1s.

9 Markarian 766 AND OTHER NLS1 GALAXIES

9.1 X–ray Emission

Markarian 766 has one of the hardest *ROSAT* spectra of the NLS1s in the sample of Boller, Brandt and Fink (1996). Indeed, some NLS1 galaxies have X–ray spectra so soft that they are quite unlike that of Markarian 766 (e.g. WPVS 007, Grupe et al. 1995, RE J1034+396, Puchnarewicz et al. 1995). It is therefore important to question whether the X–ray emission observed in the ultrasoft NLS1s could come from the same physical processes as that observed in the very much harder NLS1s like Markarian 766. Variability and spectral properties are important diagnostics; similar physical processes can be expected to produce similar spectral shapes and similar variability characteristics. The results presented here show that the X–ray spectrum of Markarian 766 has two important X–ray emission components (the power law and soft excess) which have different spectral shapes and different variability properties: a power law component which varies rapidly (thousands of seconds) and is softer when it is brighter, and a soft excess which does not exhibit any measurable rapid variability.

NLS1 galaxies which do not have extremely soft *ROSAT* spectra might be expected to be most similar to Markarian 766. The best studied of these at X–ray wavelengths are NGC4051 and MCG-6-30-15. In both these AGN the power law component shows rapid (hundreds of seconds) variability, and becomes softer as it increases in flux. This variability is found in *EXOSAT* and *GINGA* observations (Papadakis & Lawrence 1995, Matsuoka et al. 1990, Kunieda et al. 1992, Pounds, Turner & Warwick 1986), i.e. has continued for a number of years. This is exactly the behaviour found in Markarian 766.

The ultra-soft NLS1 galaxies show a more varied picture; some like RE J1034+396 show no significant rapid variability in either power law or soft excess components (Pounds, Done & Osborne 1995), while IRAS 13224-3809 (Otani et al. 1996, Boller et al. 1993) shows extremely rapid variability involving both soft excess and power law components and PHL 1092 (Forster & Halpern 1996) shows rapid variability of at least the soft excess component. Other ultra-soft objects have shown extreme variations in their soft excess over a relatively long time scale (e.g. the *ROSAT* count rate of RE J1237+264 varied by a factor of ~ 70 between two observations separated by one year with no measurable spectral change, and the *ROSAT* count rate of WPVS 007 varied by a factor of ~ 400 in one year).

Boller, Brandt & Fink (1996) concluded that NLS1s in general show considerable rapid variability, as well as softer than average *ROSAT* spectra. It has often been assumed that the variability comes from the soft excess in these objects (a natural assumption given that NLS1s as a class are unusual in showing both large soft excesses and rapid soft X–ray variability) but this is not the case for Markarian 766.

9.2 Multiwavelength Spectra

The multiwavelength spectrum of Markarian 766 is shown in Fig. 11. The largest and smallest blackbody and power law model components from the P6 *ROSAT* spectral fitting are shown as solid lines. Also shown, as dotted lines, are the power law components from the two spectral states identified in *ASCA* data by Leighly et al. (1996). The optical spectrum is taken from González-Delgado & Pérez (1996). Note that the data in this plot are not simultaneous, the optical and ultraviolet spectra have not been dereddened, and the model X–ray spectrum has not been adjusted for absorption by neutral material. Markarian 766 has a large *IRAS* bump: it emits more power from 10 - 100 microns than in the *ROSAT* energy range.

The spectrum is unusual among Seyfert 1 galaxies in that it shows no evidence for the big blue bump in the ultraviolet. This has been noticed before by Walter & Fink (1993) in that Markarian 766 has an unusually low ratio of ultraviolet to soft X–ray flux given its soft X–ray slope. Most of the Walter & Fink (1993) sample of *ROSAT* all sky survey selected Seyfert 1 galaxies fit a strong correlation between soft X–ray slope and the ratio of ultraviolet (1375 Å) to soft X–ray flux, suggesting that they have big blue bumps which rise in the UV, peak in the EUV and extend to soft X–ray energies. Besides Markarian 766, five other outliers were found by Walter & Fink (see their

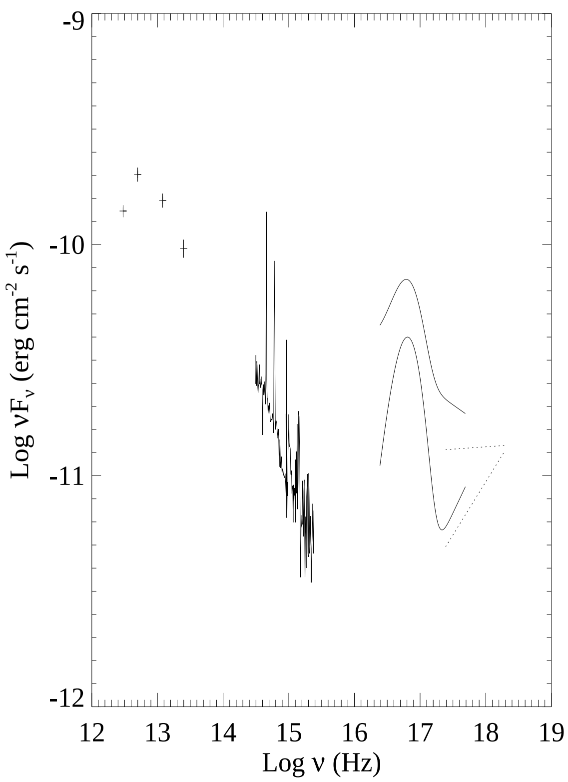

Figure 11. The multiwavelength spectrum of Markarian 766

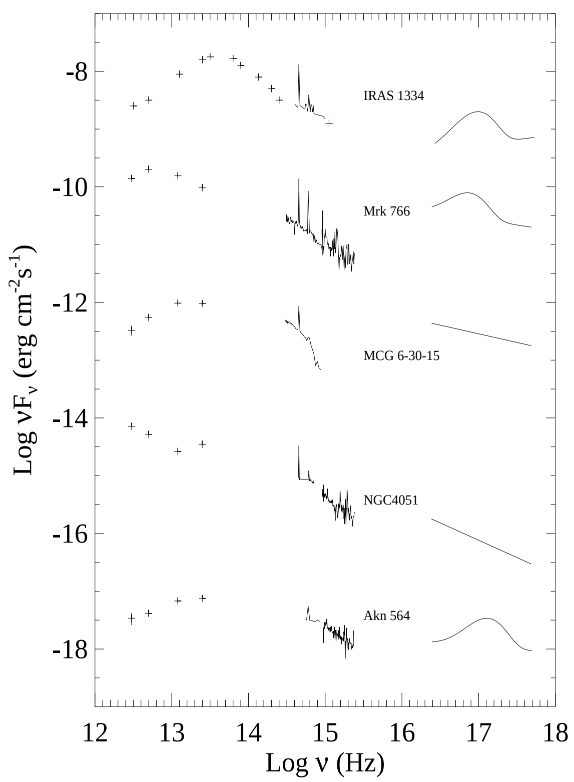

Figure 12. The multiwavelength spectra of the outlying NLS1s of Walter & Fink (1993). Note that the spectra have been vertically shifted for clarity.

figure 8), which have a low ultraviolet to soft X–ray flux ratio given their soft X–ray spectral slopes. Of these five, one is the broad line Seyfert 1 galaxy IC4329A, in which the lack of ultraviolet flux is probably caused by attenuation by dust in the edge on host galaxy. The remaining four Seyferts, Akn 564, NGC 4051, IRAS 13349+2438, and MCG-6-30-15 have Balmer lines with FWHM $<$ 2000 km s^{-1} and could all be classified as NLS1s by the criteria of Goodrich (1989). The multiwavelength spectra of these objects are plotted in Fig. 12, and sources for these data are given in Table 5. All are particularly similar to that of Markarian 766; they have very large infrared bumps and falling optical – ultraviolet spectral shapes. The lack of ultraviolet flux in these objects may be a result of their having very high temperature soft excesses, or (as suggested by Walter & Fink 1993) it may be due to reddening by dust. Although not included in the Walter & Fink sample, the ultrasoft NLS1 RE J1034+396 also exhibits a similar multiwavelength continuum shape (Puchnarewicz et al. 1995).

The outlying objects in the Walter & Fink sample are also very similar to Markarian 766 in their X–ray spectral and variability properties. NGC 4051 has a highly variable power law component which softens as it increases in flux (Papadakis & Lawrence 1995) and a soft excess blackbody component with kT $\sim$ 100 eV (Mihara et al. 1994, Pounds et al. 1994). Papadakis & Lawrence's cross correlation between the soft (0.1 - 2 keV) and hard (2 - 8 keV) flux is highly asymmetric such that the soft flux tends to lead the hard flux, and the power spectrum of the soft flux is steeper than that of the hard flux (i.e. the soft flux has more change over longer time scales) which would be consistent with a slowly varying soft excess and a rapidly varying power law component. Akn 564 shows variability by around 20% over 1500s during the *ROSAT* observations of Brandt et al. (1994), and when the soft excess is modeled as a blackbody the power law component has a similar slope ($\Gamma \sim 2.1$) and the blackbody a similar temperature (kT $\sim$ 130 eV) to Markarian 766. IRAS 13349+2438 is also variable, although as yet no rapid variability has been seen, and when the *ROSAT* spectrum is modeled as a power law and blackbody soft excess has a similar power law index ($\Gamma \sim 1.8$) and soft excess temperature (kT $\sim$ 90 eV) to Markarian 766, (Brandt et al. 1995). MCG-6-30-15 also varies rapidly (Reynolds et al. 1995), and has a hard power law component which softens as it increases in flux, although no soft excess has as yet been detected.

Brandt et al. (1994 and 1995) found no evidence for any intrinsic neutral column in *ROSAT* spectra of Akn 564 or IRAS 13349+2438, and preferred spectral models without a soft excess component because the presence of a soft excess would require a neutral column which is smaller than the measured Galactic column; their spectral fitting was based on *ROSAT* observations performed in December 1992 (IRAS 13349+2438) and November 1993 (Akn 564), with both targets at the centre of the PSPC. As discussed in Section 2.1 and Appendix A, *ROSAT* obser-

Table 5. Data sources for Fig. 12

Object	νF_ν shift	IR	Optical	X–ray
Markarian 766	0	*IRAS* *	González-Delgado & Pérez 1996	this work
IRAS 13349+2438	+2	Beichman et al. 1986	Wills et al. 1992	Brandt et al. 1996
MCG-6-30-15	-2	*IRAS* *	Morris & Ward 1988	Walter & Fink 1993
Akn 564	-7	-	Cruz-González et al. 1994	Brandt et al. 1994
NGC4051	-5	*IRAS* *	Ho, Filippenko & Sargent 1995	McHardy et al. 1995

* *IRAS* fluxes were obtained via the NASA extragalactic database (NED).
All ultraviolet data obtained from the Rutherford Appleton IUE archive.

vations made around these times with the target at the centre of the PSPC were particularly affected by the PSPC temporal/spatial gain variation. Without the recalibration software now available, the most marked effect is that the fitted absorbing column is underestimated. Even with an edge to represent absorption from O VII and O VIII, the underlying spectra in these two objects are unusually steep ($\Gamma > 2.5$), suggesting that they *do* have soft excesses.

The very similar multiwavelength spectra and X–ray properties in these objects probably mean that they lack ultraviolet flux for a common reason.

Attributing the lack of ultraviolet flux to reddening by dust in the line of sight is an attractive solution. Optical polarization of Markarian 766, of $\sim 2\%$ increasing to the blue, indicates scattering from dust grains. These dust grains are probably located within the narrow line region, because the broad lines show more polarization than the narrow lines (Goodrich 1989). For Markarian 766, the required amount of reddening to make the ultraviolet flux match the Walter & Fink (1993) ultraviolet – soft X–ray relation is consistent with its high Balmer decrement ($H_\alpha/H_\beta = 5.1$) seen in the optical spectrum. This amount of reddening is about twenty times that expected for a Galactic gas to dust ratio and the measured cold absorbing column of $\sim 3 \times 10^{20}\mathrm{cm}^{-2}$ (Walter & Fink 1993). This is reasonable if the dust is located in the narrow line region where hydrogen and helium will be predominantly ionized. The cross section for photoelectric absorption by metals in dust grains can be much smaller than for metals in the gas phase because of self blanketing (e.g. Fireman 1974 states that the 0.3 keV photoelectric cross section for 0.6 μ radius dust grains is only $\sim 20\%$ its value for gaseous metals.) Similar conclusions can be drawn from polarization properties and Balmer decrements of IRAS 13349+2438 and MCG-6-30-15 (Wills et al. 1992, Thomson & Martin 1988).

Thermal emission from dust is also probably the best explanation of the large *IRAS* bumps in these objects. A large excess of 10 - 100 micron emission appears to be a common property in many NLS1 galaxies, including those which are ultrasoft such as RE J1034+396 (Puchnarewicz et al. 1995). Detailed sub-millimetre observations of the NLS1 1Zw1 indicate that the IRAS bump is well fitted by thermal emission from dust, but is poorly fitted by synchrotron models (Hughes, et al. 1993). The evidence for dust in these objects is extremely strong, *even if* the deficit of ultraviolet flux is related to unusually high big blue bump temperatures.

It is therefore likely that dusty Seyfert 1 galaxies are preferentially those which have narrow lines. This is supported by the fact that the only five Seyfert 1s of the Walter & Fink (1993) sample to show evidence for dust reddening have narrow lines. It is further supported by the large ratio of narrow to broad line Seyfert 1s found in *IRAS* surveys (> 20% in the *IRAS* samples of Spinoglio & Malkan 1989 and Osterbrock & DeRobertis 1985) and small ratio ($\sim$ 10%) of narrow to broad line Seyfert 1s found in optical surveys (Stephens 1989).

Finally, in the unified model for AGN, Seyfert 2 galaxies are Seyfert 1 galaxies viewed side-on, such that the broad line regions are obscured from us. The hidden broad line regions (and Seyfert 1 type optical continua) of Seyfert 2 galaxies can be seen in polarized light. This is scattered into our line of sight by free electrons, which scatter optical light more or less independently of wavelength, or dust, which scatters blue light much more than red light (Antonucci 1993). If more dust is found beyond the broad line region in NLS1s than in broad line Seyfert 1s, we would expect those Seyfert 2s which have the largest red-blue polarization gradient to have hidden broad line profiles like those of NLS1s. The numbers and qualities of spectropolarimetric observations of Seyfert 2 galaxies are not sufficient to address this issue quantatively, but this hypothesis is qualitatively supported: of the Miller & Goodrich (1990) sample of eight highly polarized Seyfert 2 galaxies, one (NGC7674) has NLS1 width polarized broad Hα and Hβ components, and this object also has the highest red-blue polarization gradient.

10 CONCLUSIONS

We have examined the variable soft X–ray emission of Markarian 766 using hardness ratios and spectral analysis of 9 *ROSAT* datasets. The spectrum is well described by a power law and a blackbody (kT $\sim$ 70 eV) soft excess. Modeling of 31 spectra at different count rates and from different observations is consistent with a variable power law component, which is softer when it is brighter, and an unchanging black body soft excess. Hardness ratios and variability amplitudes in three energy bands are in agreement with this picture, showing that the power law component varies continuously on a time scale of $\sim$ 5000s but the soft excess component probably does not vary significantly within the observations. This variability can be explained if the power law is produced by thermal or non-thermal Comptonization of soft photons. While pair reprocessing could produce the correlation between power law spectral index and flux, delays expected between changes in the hard and soft flux are not seen.

The behaviour of Markarian 766 is highly analogous to that of Galactic black hole candidates in the low state, which have rapidly variable power law components and less variable (extended) soft excesses.

The time scale for variation in the *ROSAT* band probably provides an upper limit for the size of the region in which the power law (but not necessarily the soft excess) is produced. This means that the physical size of the soft excess region may be much larger than the X–ray power law producing region, and hence is consistent with the soft excess having similar variability time scales to the ultraviolet part of the big blue bump.

Markarian 766 is known to have a deficit of ultraviolet flux relative to its X–ray emission. We show that the four other objects in the Walter & Fink (1993) sample of *ROSAT* all sky survey selected Seyfert 1 galaxies, which show a lack of ultraviolet emission (excluding IC4329a which is probably strongly absorbed by its edge-on host galaxy) have very similar infrared to X–ray flux distributions to Markarian 766. These galaxies could all be classed as NLS1s, and are seen to have very similar X–ray spectral and variability properties to Markarian 766 (calibration uncertainties in the *ROSAT* PSPC mean that two of these objects, IRAS 13349+2438 and Ark 564, may be more like Markarian 766 than was previously thought). We argue that the multiwavelength flux distributions of these objects support the Walter & Fink suggestion that the ultraviolet flux deficit is related to dust extinction, and show that other independent data are consistent with a picture in which NLS1s have more dust in their narrow line regions than broad line Seyfert 1s.

11 ACKNOWLEDGMENTS

MJP acknowledges the support of a PPARC studentship throughout much of this work. Partial financial support for FJC was provided by the DGES under project PB95-0122. This research has made use of data obtained from the Leicester Database and Archive Service at the Department of Physics and Astronomy, Leicester University, UK. This research has made use of the NASA/IPAC Extragalactic Database (NED) which is operated by the Jet Propulsion Laboratory, California Institute of Technology, under contract with the National Aeronautics and Space Administration.

12 REFERENCES

Antonucci R., 1993, Annu. Rev. Astron. Astrophys., 31, 473

Beichman C.A., Soifer B.T., Helou G., Chester T.J., Neugebauer G., Gillett F.C., Low F.J., 1986, ApJ, 308, L1

Boller Th., Brandt W.N. and Fink H.H., 1996 A&A, 305, 53

Boller Th., Trümper J., Molendi S., Fink H., Schaeidt S., Caulet A., Dennefeld M., 1993, A&A, 279, 53

Brandt W.N., Fabian A.C., Nandra K., Reynolds C.S., Brinkmann W., 1994, MNRAS, 271, 958

Brandt W.N., Fabian A.C. and Pounds K.A., 1996, MNRAS, 278, 326

Brandt W.N., Pounds K.A., Fink H., 1995, MNRAS, 273, L47

Cruz-Gonzalez I., Carrasco L., Serrano A., Guichard J., Dultzin-Hacyan D., Bisiacchi G. F., 1994, ApJS, 94, 47

Done C., Fabian A.C., 1989, MNRAS, 240, 81

Done C., Fabian A.C., Ward M.J. Kunieda H., Tsuruta S., 1990, MNRAS, 243, 713

Done C., Madejski M., Mushotzky R.F., Turner T.J., Koyama K., Kunieda H., 1992a, ApJ, 400, 138

Done C., Mulchaey J.S., Mushotzky R.F., Arnaud K.A., 1992b, ApJ, 395, 275

Ebisawa K., Titarchuk L., Chakrabarti S.K., 1996, PASJ, 48, 59

Edelson R.A. and Krolik J.H., 1988, ApJ, 333, 646

Edelson R.A., 1992, ApJ, 401, 516

Fireman E.L., 1974, ApJ, 187, 57

Forster K., Halpern J.P., 1996, ApJ, 468, 565

Gonzalez Delgado R.M. & Perez E., 1996, MNRAS, 278, 737

Goodridge R.W., 1989, ApJ, 342, 224

Grupe D., Beuerman K., Mannheim K., Thomas H.-C., Fink H.H., de Martino D., 1995, A&A, 300, L21

Guilbert P.W. and Rees M.J., 1988, MNRAS, 233, 475

Hasinger G., Boese G., Predehl P., Turner T.J., Yusaf R., George I.M., Rohrbach G., 1994a, MPE/OGIP Calibration Memo CAL/ROS/93-015

Hasinger G.H., Prieto A., Snowden S., 1994b, MPE *ROSAT* Newsletter issue 10,

Ho L.C., Filippenko A.V. & Sargent W.L., 1995, ApJS, 98, 477

Hughes D.H., Robson E.I., Dunlop J.S., Gear W.K., 1993, MNRAS, 263, 607

Kunieda H., Hayakawa S., Tawara Y., Koyama K., Tsusaka Y., Leighly K., 1992, ApJ, 384, 482

Lawson A.J., Turner M.J.L., Williams O.R., Stewart G.C., Saxton R.D., 1992, MNRAS, 259, 743

Leighly K.M., Mushotzky R.F., Yaqoob T., Kunieda H., Edelson R., 1996, ApJ, 469, 147

Matsuoka M., Piro M., Yamauchi M., Murakami T., 1990, ApJ, 361, 440

McHardy I.M., Green A.R., Done C., Puchnarewicz E.M., Mason K.O., Branduardi-Raymont G., Jones M.H., 1995, MNRAS, 273, 549

Miller J.S. & Goodrich R., 1990, ApJ, 355, 456

Mihara T., Matsuoka M., Mushotzky R.F., Kunieda H., Otani C., Miyamoto S., Yamauchi M., 1994, PASJ, 46, 137

Miyamoto S. & Kitamoto S., 1989, Nature, 342, 773

Molendi S., Maccacaro T. and Schaeidt S., 1993, A&A, 271, 18

Molendi S. and Maccacaro T., 1994, A&A, 291, 420

Morris S.L. & Ward M.J., 1988, MNRAS, 230, 639

Nandra K., George I.M., Mushotzky R.F., Turner T.J., Yaqoob T., 1997, ApJ, 477, 602

Netzer H., Turner T.J. and George I.M., 1994, ApJ, 435, 106

Osterbrock D.E. & DeRobertis M.M., 1985, PASP, 97, 902

Otani C., Tsuneo K., Kayoko M., 1996, MPE Report 263,

'Rontgenstrahlung from the Universe', Zimmermann U., Trumper J.E., Yorke H. (eds)
Papadakis I.E., & Lawrence A., 1995, MNRAS, 272, 161
Pounds K.A., Done C., Osborne J.P., 1995, MNRAS, 277, 5P
Pounds K.A., Nandra K., Fink H.H. and Makino F., 1994, MNRAS, 267, 193
Pounds K.A., Nandra K., Stewart G.C., George I.M., Fabian A.C., 1990, Nature, 344, 132
Pounds K.A., Turner T.J., Warwick R.S., 1986, MNRAS, 221, 7P
Prieto M.A., Hasinger G., Snowden S., 1994, MPE Calibration Memo TN-ROS-MPE-ZA00/032
Puchnarewicz E.M., Mason K.O., Cordova F.A., Kartje J., Branduardi-Raymont G., Mittaz J.P.D., Murdin P.G., Allington-Smith J., 1992, MNRAS, 256, 589
Puchnarewicz E.M., Mason K.O., Siemiginowska A., Pounds K.A., 1995, MNRAS, 276, 1281
Reynolds C.S., Fabian A.C., Nandra K., Inoue H., Kunieda H., Iwasawa K., 1995, MNRAS, 277, 901
Ross R.R., Fabian A.C. and Mineshige S., 1992, MNRAS, 258, 189
Ross R.R. and Fabian A.C., 1993, MNRAS, 261, 74
Shastri P., Wilkes B.J., Elvis M., McDowell J., 1993, ApJ, 410, 29
Snowden S.L., McCammon D., Burrows D.N. and Mendenhall J.A., 1994, ApJ, 424, 714
Snowden S.L., Turner T.J., George I.M., Yusaf R., Predehl P., Prieto A., 1995, OGIP Calibration Memo CAL/ROS/95-003
Spinoglio L. & Malkan M.A., 1989, ApJ, 342, 83
Stark A.A., Gammie C.F., Wilson R.W., Bally J., Linke R., Heiles C., Hurwitz M., 1992, ApJS, 79, 77
Stephens A.J., 1989, 97, 10
Svensson R., 1987, MNRAS, 227, 403
Tanaka Y., Nandra K., Fabian A.C., Inoue H., Otani C., Dotani T., Hayashida K., Iwasawa K., Kii T., Kunieda H., Makino F., Matsuoka M., 1995, Nature, 375, 659
Thompson I.B., Martin P.G., 1988, ApJ, 330, 121
Torricelli-Ciamponi G. & Courvoisier T.J.-L., 1995, A&A, 296, 651
Turner T.J., 1993, OGIP Calibration Memo CAL/ROS/93-007
Turner T.J., Pounds K.A., 1989, MNRAS, 240, 833
Walter R., & Courvoisier T.J.-L., 1992, A&A, 266, 65
Walter R. & Fink H.H., 1993, A&A, 274, 105
Wills B.J., Wills D., Evans N.J., Natta A., Thompson K.L., Breger M., Sitko M.L., 1992, ApJ, 400, 96
Zdiarzki A.A., Ghisellini G., George I.M., Svensson R., Fabian A.C., Done C., 1990, ApJ, 363, L1

A The *ROSAT* PSPC gain drift and the Markarian 766 data

In Section 2.1 we stated that observations P4, P8 and P9 are probably most affected by the PSPC spatial/temporal gain drift. It *is* known that there has been a significant change in response *on-axis* between the beginning and end of the PSPC lifetime (Snowden et al. 1995). The latest information (M.J. Freyberg et al. 1996, *http://wave.xray.mpe.mpg.de/rosat /calibration/pspc/PSPC_cal_status.html*) is that large residuals are found in bright, on-axis sources observed later than mid 1992. From this one would expect observations P4, P8 and P9 to be affected by the gain drift; it is unclear whether observation P2 should be affected as well. Software to correct for this gain variation is now available in the form of the PCPICOR task in FTOOLS and PROCESS/CT in EXSAS, but because the investigation reported here was begun before this software was generally available, it was initially performed without this correction. The difference between the corrected and uncorrected spectra is considerable.

The most noticeable difference concerns the soft end of the P4, P8 and P9 spectra: before correction with PCPICOR they all had smaller fitted absorption and higher black body temperatures, (e.g. for comparison with model B in Table 3, P4, P8 and P9 had best fit columns of 1.7, 1.8 and 2.0 $\times 10^{20}\mathrm{cm}^{-2}$ and best fit black body temperatures of 99, 87 and 105 eV respectively). As an illustration of this difference we show the pre and post PCPICOR residuals of a power law fit assuming Galactic N_{H} to the P9 data in Fig. A1 and Fig. A2. Note how different the pre-correction residuals are to those for the P2 observation shown earlier (Fig. 4). The offaxis observation P5 was affected in the opposite sense by PCPICOR, in that the fitted column decreased after correction.

However, despite the improvement that PCPICOR makes, the three on-axis observations *still* have lower fitted columns and higher fitted temperatures than the most of the other observations, suggesting they may still have calibration differences which are significant in data of this signal to noise. The scatter of fitted temperatures and columns in Table 3 is of the same order as the differences made by PCPICOR; we therefore consider that the different fitted temperatures and columns for the different observations could be due to remaining PSPC calibration uncertainties.

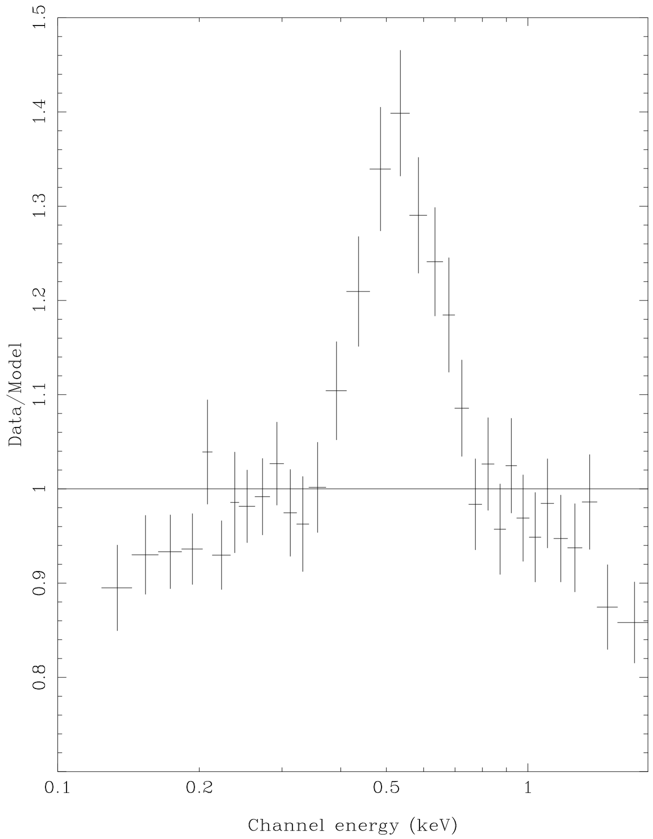

Figure A1 Ratio of a power law model (best fit $\Gamma = 2.2$) with fixed Galactic $N_{\rm H}$, to the P9 spectrum *before* correction using PCPICOR. Note that the residuals are found at higher energies than for the P2 spectrum shown in Fig. 4.

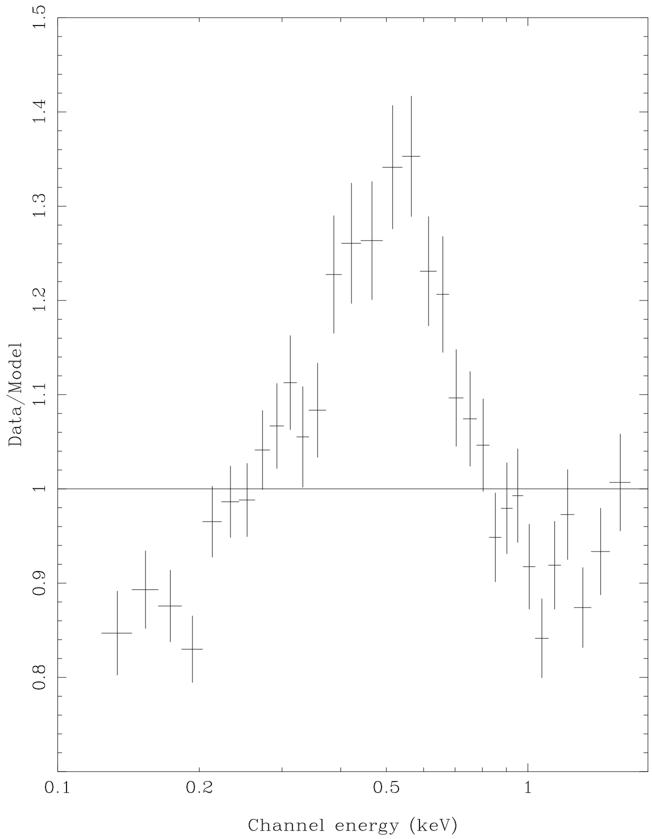

Figure A2 Ratio of a power law model (best fit $\Gamma = 2.2$) with fixed Galactic $N_{\rm H}$, to the P9 spectrum *after* correction with PCPICOR. Note that the residuals now have a similar shape to those in Fig. 4